

Design and Construction of a Variable Temperature Atomic Force Microscope

By

Bethany J. Little

A thesis submitted in partial fulfillment of the requirements for
the degree of

Bachelor of Science

Houghton College

May 2009

Signature of Author

Department of Physics
May 5, 2009

.....

Dr. Brandon Hoffman
Assistant Professor of Physics
Research Supervisor

.....

Dr. Mark Yuly
Professor of Physics

Design and construction of a Variable temperature Atomic Force Microscope

By

Bethany J. Little

Submitted to the Houghton College Department of Physics
on May 5, 2009 in partial fulfillment of the requirement for
the degree of Bachelor of Science

Abstract

A variable temperature atomic force microscope is being constructed at Houghton College. The microscope will operate in a rough vacuum and will utilize spring vibration isolation and eddy current damping to minimize mechanical vibration. A modified “Johnny Walker” beetle is being constructed for the rough approach. The sample will be mounted onto the walker scanning head and scanned across a cantilever tip and laser assembly. When completed, resolution should be on the order of nanometers. Liquid nitrogen and resistive heating will allow operation from ~ 100 K to 500 K.

Thesis Supervisor: Dr. Brandon Hoffman

Title: Assistant Professor of Physics

TABLE OF CONTENTS

TABLE OF FIGURES	5
Chapter 1 HISTORY AND MOTIVATION.....	7
1.1 Introduction	7
1.2 Precursors to the AFM.....	7
1.2.1 The Profiler	7
1.2.2 The Topografiner.....	7
1.2.3 The STM.....	8
1.3 The First AFM	9
1.4 Taking the AFM a step further.....	10
Chapter 2 THEORY	11
2.1 Introduction	11
2.2 Cantilevers	11
2.3 Forces	12
2.3.1 Van Der Waals Forces	12
2.3.2 Lateral Forces	17
2.3.3 Capillary Forces	19
2.4 Modes of Operation	19
2.4.1 Contact Mode	19
2.4.2 Vibrating Mode	20
2.5 Tip Geometry Effects.....	21
2.6 Tip Characterization	23
2.7 Measurement of the Oscillations of the Cantilever	24
2.8 Sources of Noise.....	26
2.9 Thermal Effects.....	26
2.9.1 Thermal Noise of the Cantilever.....	26
2.9.2 Thermal Expansion of different materials	27
2.9.3 Thermal Effects on the Cantilever Due to the Laser.....	28
2.10 Piezoelectric crystals	28
2.10.1 The Piezoelectric Effect.....	28
2.10.2 Sources of Error	29
2.10.3 “Stick-Slip” Theory of Approach.....	30
Chapter 3 A VARIABLE TEMPERATURE AFM.....	31

3.1	Model.....	31
3.2	Overall Design.....	31
3.3	Damping System.....	31
3.4	Movement of the Sample	33
3.4.1	Positioning of the Sample	33
3.4.2	Scanning of the Sample.....	34
3.5	Oscillations of the Cantilever.....	35
3.6	Heating and Cooling	36
3.7	LabVIEW Program	36
3.7.1	The Approach Sub-Program	37
3.7.2	The Positioning Sub-Program.....	38
3.7.3	Scanning Sub-Program	39
3.7.4	Future Work on the LabVIEW Program.....	40
3.8	Electronics.....	40
3.8.1	Signal Conversion Circuit.....	41
3.8.2	Amplification Circuits	42
Chapter 4	CONCLUSION	48
4.1	Summary.....	48
4.2	Future Work	48
Appendix	LABVIEW PROGRAM.....	49
4.3	Introduction	49
4.4	Menu.vi.....	49
4.5	Approach.vi	54
4.6	Positioning.vi	57
4.7	Scanning	63
REFERENCES	65

TABLE OF FIGURES

Figure 1. Explanation of field emission.....	8
Figure 2. Schematic diagram of the first AFM, a modified STM.....	9
Figure 3. A cantilever with a tip at one end and fixed at the other end.....	11
Figure 4. Two spherical particles used in the derivation of the macroscopic Van der Waals Force.	15
Figure 5. Geometric model of the tip and sample.....	17
Figure 6. The cantilever is modeled as a rod of length L , height h and width w	18
Figure 7. Front view of the cantilever and tip, showing the direction of the lateral forces.....	19
Figure 8. Schematic of an AFM.....	20
Figure 9. Two different tip shapes create different images of a grooved sample.....	21
Figure 10. The image of the surface is directly related to the angle which defines the pointed tip.	22
Figure 11. Further changes in tip geometry affect the image.....	22
Figure 12. Diagram of a laser deflection system, including a four-quadrant detector.....	24
Figure 13. The interferometric detection system.....	25
Figure 14. Diagram of a cylindrical piezoelectric ceramic.....	29
Figure 15. The three steps of stick-slip motion are shown.....	30
Figure 16. Schematic diagram of the AFM (not to scale).	32
Figure 17. Diagram of the damping system.....	33
Figure 18. Illustration of the voltage function used for scanning.....	35
Figure 19. Design of the cantilever driver.....	36
Figure 20. Logic diagram for the “approach” sub-program.....	37
Figure 21. Logic diagram for the main event cases in the Positioning program.	39
Figure 22. Logic diagram of the function of the electronics in the AFM.....	41
Figure 23. Diagram of DAC circuit.	42
Figure 24. Circuit diagram for EMCO C20 High voltage supply.....	42
Figure 25. Circuit diagram for scanning.	43
Figure 26. Overhead views of the sample mount, for scanning motion.....	44
Figure 27. Overhead view of the sample mount, geometry.	45

Figure 28. Overhead view of the sample mount, for circular motion	46
Figure 29. Schematic of the approach circuit	47
Figure 30. Front panel for Menu.vi.....	49
Figure 31. Block diagram for Menu.vi	50
Figure 32. Event case for the Menu.vi: timeout.	50
Figure 33. Event case for the Menu.vi: opens Scanner program	51
Figure 34. Event case for the Menu.vi: opens Drive program.....	51
Figure 35. Event case for the Menu.vi: opens Approach program.....	51
Figure 36. Event case for the Menu.vi: text strings.....	52
Figure 37. Event case for the Menu.vi: stop.....	53
Figure 38. Front panel for the approach sub program, Approach.vi.	54
Figure 39. Block diagram for Approach.vi.	55
Figure 40. Cycle subvi.....	56
Figure 41. Front panel for Positioning.vi.....	57
Figure 42. Block diagram for Positioning.vi.....	58
Figure 43. Event case for Positioning.vi: timeout.	59
Figure 44. Event case for Positioning.vi: program end.....	59
Figure 45. Event case for Positioning.vi: calibration	60
Figure 46. Event case for Positioning.vi: motion in the negative x direction.	60
Figure 47. Event case for Positioning.vi: motion in the positive x direction.	61
Figure 48. Event case for Positioning.vi: motion in the negative y direction.	61
Figure 49. Event case for Positioning.vi: motion in the positive y direction	62
Figure 51. Front panel for Scanning.vi.....	63
Figure 52. Block diagram for Scanning.vi.	64

Chapter 1

HISTORY AND MOTIVATION

1.1 Introduction

Ever since the limits of optical microscopy were reached, other methods have been devised to probe the nature of matter on smaller scales. One such device is the atomic force microscope (AFM), originally developed in 1985 by Binnig, Quate and Gerber [1]. It enabled atomic resolution of surface topography and was useful in mapping out the atomic interactions between the sample and the tip. An overview of the history of the AFM reveals the great use of this device and lends insight into the reasons for the building of the particular device of this project.

1.2 Precursors to the AFM

1.2.1 *The Profiler*

One early alternative to the optical microscope was the profiler, invented in 1929 [2], which was used for measuring the vertical features on a surface. A sample was dragged across a cantilever tip which was mounted on a flexible joint. Vertical features in the surface would cause the cantilever to move up and down. The movement of the cantilever could be measured using reflected light. The downside to this method was the potential damage to both the tip and the sample caused by contact.

1.2.2 *The Topografiner*

In 1972 Young, Ward and Scire [3] described the first non-contact scanner, which they called a topografiner. They accomplished this using field emission. Field emission is the extraction of electrons from a material through application of an electric field, as shown in Figure 1. This field effectively decreases the barrier for tunneling of these electrons from the surface. Young *et. al.* mounted a tungsten emitter on piezo ceramics. The potential on these ceramics was controlled by the field emission current; thus a constant distance could be maintained between the tip and sample. Vibrations limited how close the sample could be to the tip, limiting the resolution to 30Å vertically and 200Å horizontally.

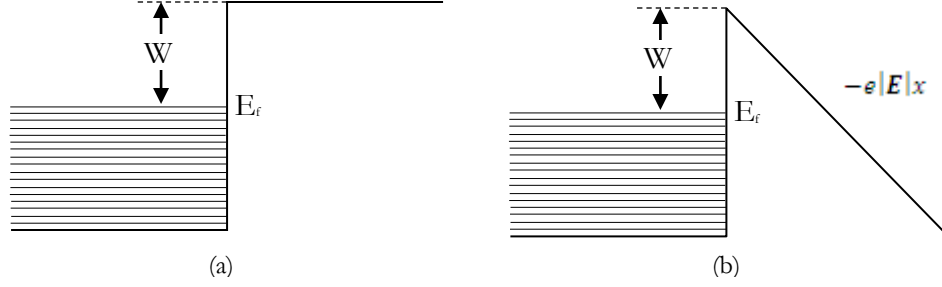


Figure 1. Field emission allows electrons to tunnel out of a material by application of an electric field. (a) With no electric field, electrons at the Fermi energy must overcome the work function W in order to leave the material. (b) A field \mathbf{E} changes the shape of the potential well, allowing electrons to tunnel through the barrier. Image from [4].

1.2.3 The STM

The scanning tunneling microscope (STM) increased the resolution of the topografiner by orders of magnitude and was crucial to the development of the AFM. The development of the STM in 1982 [5] allowed the mapping of individual atoms on a conductive surfaces. Binnig and Rohrer [5] were able to decrease the noise so that, in their STM, the distance between the tip and sample could be 10\AA , enabling them to and use the quantum mechanically predicted effect called tunneling. A conductive tip with a radius of curvature on the order of 10\AA was brought within 10\AA of a conductive sample in a vacuum. The vacuum between the tip and the sample served as the barrier to tunneling. The tunneling current J_T between two electrodes with an applied voltage V_T and average work function ϕ is proportional to the distance s between the electrodes by the relationship [5]

$$J_T \propto \frac{V_T}{s} e^{-A\sqrt{\phi}s} \quad (1)$$

where $A \approx 1.025 (\text{eV})^{-1/2} \text{\AA}^{-1}$. Thus we can see that, for work functions of only a few eV, the current changes by an order of magnitude for only an angstrom change in the distance between the electrodes [5]. This allows high resolution vertical imaging of the sample. The sharpness of the tip enables high resolution on the lateral scale. Using this method, Binnig and Rohrer [5] were able to see the rhombohedral unit cells on a piece of silicon and resolve atoms on the surface.

1.3 The First AFM

Since the operation of the STM depends on the motion of electrons in the surface of the sample, further developments would be required for the imaging of insulators on this scale to be made possible. In 1985, an STM was modified by Binnig, Quate and Gerber [1] to measure the oscillations of a cantilever with a tip on it, as shown in Figure 2. As the tip was brought close to the sample, interatomic forces affected the phase and amplitude of the oscillations. The STM tip was used to measure these oscillations. They experimented with different modes of operation, and found that it worked best if the tunneling current between the STM and the cantilever was kept constant, with one feedback loop maintaining a constant distance between the tip and the sample. They also found that imaging of the sample was optimized when the tip and the sample were oscillated, in opposite directions. Shortly after its invention, the AFM was used to “show atomic corrugations with a lateral resolution better than 3 Å” [6].

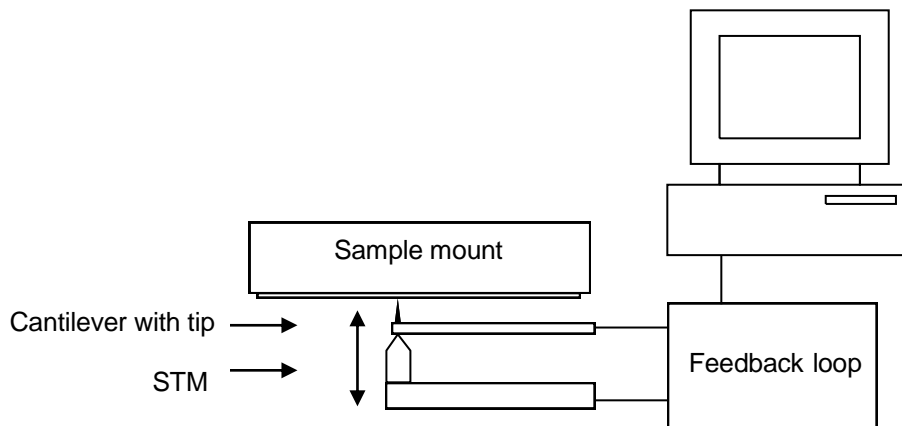


Figure 2. Schematic diagram of the first AFM, a modified STM. The STM is used to monitor the oscillations of the cantilever tip. The phase and amplitude of the cantilever change as the tip comes close to the sample. A feedback loop moves the STM and cantilever up and down so that the tip is kept at a constant distance from the sample as it scans.

1.4 Taking the AFM a step further

Since AFMs are so useful, they have been developed to the point that they are now commercially available. However, these available AFMs have limitations. This project aims to overcome one of these limitations by building a variable temperature AFM, which would allow surfaces to be studied at different temperatures and even during temperature change.

Much can be learned about a material by watching its behavior as it undergoes temperature changes. For example, during temperature change, different grains may form, with the preference for grains of certain orientations dependent on temperature. Since the AFM is able to provide detailed information about a surface, it would be very useful if surfaces could be observed during temperature change. It is for this reason that we have chosen to build a variable temperature AFM.

Chapter 2

THEORY

2.1 Introduction

There are many different areas of knowledge that make the building of an AFM possible. Cantilevers and the forces acting on them must be well understood. The measuring process, including the modes of operation, tip shape effects, and measurement technique, should also be considered. Sources of noise must also be examined, especially with regard to thermal effects and the use of piezo electric crystals. This chapter will explore the theory behind each of these areas in order to provide the necessary background for the specific details of this project.

2.2 Cantilevers

Arguably the most important part of the AFM, the cantilever must be well understood. Recently, a comprehensive study [7] has been done which models the cantilever by including four major factors: rotary inertia of the beam, sheer deformation of the beam, mass of the tip, and rotary inertia of the tip. The results of this study, while useful as a point of reference and helpful to engineers of these tips, need only be considered in the case where the mass ratio of the tip to the cantilever is high. For the purposes of this paper, the cantilever will be modeled as a simple harmonic oscillator. The cantilever is made of flexible material so that a force applied to one end causes it to bend, as shown in Figure 3.



Figure 3. A cantilever with a tip at one end and fixed at the other end. The displacement x of the end of the lever is directly proportional to the force on the tip.

The displacement x is proportional to the magnitude of the force acting on the cantilever by a proportionality constant K , so that

$$F = -Kx \quad (2)$$

Using Newton's second law, $\sum F = ma = m \frac{d^2x}{dt^2}$, we have

$$m \frac{d^2x}{dt^2} = -Kx. \quad (3)$$

Let

$$\omega_o = \sqrt{\frac{K}{m}} \quad (4)$$

so that

$$\frac{d^2x}{dt^2} = -\omega_o^2 x. \quad (5)$$

This is a differential equation that will have a solution of the form

$$x = A \sin \omega_o t + B \cos \omega_o t, \quad (6)$$

where A and B are constants.

From this we can see that the cantilever will oscillate with angular resonant frequency ω_o , which, according to Equation 4, is directly proportional to the spring constant of the material and inversely proportional to the mass. Thus a stiff (high k) and light (low m) cantilever would have a high resonant frequency, while a more flexible and heavier cantilever would have a much lower resonant frequency. In an AFM, where the cantilever is driven at its resonance frequency, a higher resonant frequency is desired. The higher frequency decreases vibrational noise (which tends to be lower in frequency) and allows for more time efficient imaging.

2.3 Forces

2.3.1 Van Der Waals Forces

The forces between the tip and the sample in an AFM are primarily in the realm of the Van der Waals force (or the London dispersion force), making a discussion of this force useful.

2.3.1.1 The Force between Two Particles

The derivation of this force begins with the analysis of the force between two particles. Beiser [8] explains how this attractive force depends on the dipole moment of particles.

Polar molecules are attracted to each other because of their magnetic moments. Polar molecules can also induce an electric field in other non-polar molecules. The electric field of a dipole is given by

$$\mathbf{E}_d = \frac{1}{4\pi\epsilon_0} \left[\frac{\mathbf{p}}{r^3} - \frac{3(\mathbf{p} \cdot \mathbf{r})}{r^5} \mathbf{r} \right]. \quad (7)$$

The electric dipole moment induced in a non-polar molecule would be proportional to \mathbf{E}_d by proportionality constant, so that $\mathbf{p}' = \alpha \mathbf{E}_d$, where α is the polarizability of the material.

The induced field has potential energy

$$\begin{aligned} \mathbf{U} &= -\mathbf{p}' \cdot \mathbf{E}_d \\ \mathbf{U} &= -\alpha \mathbf{E}_d \cdot \mathbf{E}_d \end{aligned} \quad (8)$$

which, in terms of the distance r , becomes

$$U = -\frac{\alpha}{(4\pi\epsilon_0)^2} \left(\frac{p^2}{r^6} \right) (1 + 3 \cos^2 \theta) \quad (9)$$

where θ is the angle between \mathbf{p} and \mathbf{r} . The force due to this field would thus be

$$F = -\frac{dU}{dr} = -6 \frac{\alpha}{(4\pi\epsilon_0)^2} \left(\frac{p^2}{r^7} \right) (1 + 3 \cos^2 \theta). \quad (10)$$

From this two things can be noted. First, since the force is negative, it is attractive. Secondly, the force is inversely proportional to r^7 , making it negligible on large distance scales, but important in the range of the AFM.

Van der Waals forces also act between non-polar molecules. In these molecules, the charge is, on average, distributed evenly. However, at any given point in time, this charge distribution fluctuates, creating a temporary dipole moment. This fluctuation induces similar changes in nearby molecules,

creating electric fields. Thus while the average dipole moment $\langle p \rangle$ is equal to zero, the average of the square of the moment, $\langle p^2 \rangle$ is not. This gives rise to Van der Waals interactions between non-polar molecules.

2.3.1.2 The Force between the Tip and the Sample

The Van der Waals force between the tip and the sample is caused by the interactions between a collection of molecules in the tip and a collection of molecules in the sample. These molecules are arranged in a specific geometry, which must be considered in order to calculate the force between tip and sample.

The geometry of the sample and the tip can be modeled as an infinite plane (the sample) and a sphere. Hamaker [9] calculated the Van der Waals force between two macroscopic spherical bodies of uniform density. If we let one of the particles have infinite radius, this is the same as the force between a sphere and an infinite plane. Hamaker began by considering that the energy of interaction between two spheres of density q atoms per cm^3 and with volume elements v_1 and v_2 is given by

$$U = - \int_{v_1} dv_1 \int_{v_2} dv_2 \frac{q^2 \lambda}{r^6} \quad (11)$$

Where λ is called the Van der Waals constant, simplifying Equation (9). Hamaker then proceeded to integrate to find the energy of interaction between two spherical masses of radius R_1 and R_2 and separated by a distance d as shown in Figure 4.

After some calculus and algebra, he arrived at the result

$$U = -\pi^2 q^2 \lambda \frac{1}{6} \left\{ \frac{2R_1 R_2}{C^2 - (R_1 + R_2)^2} + \frac{2R_1 R_2}{C^2 - (R_1 - R_2)^2} + \ln \frac{C^2 - (R_1 + R_2)^2}{C^2 - (R_1 - R_2)^2} \right\}, \quad (12)$$

which can be simplified by substituting in $C=R_1 + R_2 + d$ and by defining

$$x = \frac{d}{2R_1} \text{ and } y = \frac{R_2}{R_1}. \quad (13)$$

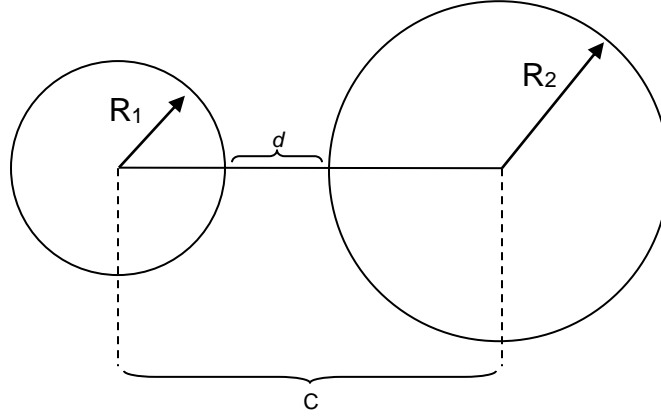


Figure 4. Two spherical particles of radii R_1 and R_2 are separated by a center-to-center distance C and nearest distance d .

Thus

$$U = -\pi^2 q^2 \lambda \frac{1}{12} \left\{ \frac{y}{x^2+xy+x} + \frac{y}{x^2+xy+x+y} + 2 \ln \frac{x^2+xy+x}{x^2+xy+x+y} \right\}. \quad (14)$$

In the case where the radius of the second sphere is infinite ($y = \infty$) we have

$$U_\infty = -\pi^2 q^2 \lambda \frac{1}{12} \left\{ \frac{1}{x} + \frac{1}{x+1} + 2 \ln \frac{x}{x+1} \right\}. \quad (15)$$

If the sphere is very close to the surface (d is small compared to R_1 , so $x \ll 1$),

$$U_\infty = -\pi^2 q^2 \lambda \frac{1}{12x}. \quad (16)$$

The force between these particles can be found by taking the derivative, as done in Equation (10).

This yields

$$F_{\infty} = -\frac{\pi^2 q^2 \lambda}{2R_1} \frac{1}{12} \left\{ \frac{2}{x} - \frac{1}{x^2} - \frac{2}{x+1} - \frac{1}{(x+1)^2} \right\}. \quad (17)$$

For the case of $x \ll 1$,

$$F_{\infty} = \frac{\pi^2 q^2 \lambda}{24R_1} \frac{1}{x^2} = \left(\frac{\pi^2 q^2 \lambda}{2} \right) \left(\frac{R_1}{6d^2} \right). \quad (18)$$

Argento and French [10] argue that these simple geometries are inadequate, and have developed a method of integration for more complex and realistic geometries. They modeled the tip as a combination of cylinder, conic section, and spherical cap, as shown in Figure 5. The resulting force, as a function of the distance d between the tip and the sample is given by:

$$F_z(d) = \frac{AR^2(1-\sin\gamma)(R\sin\gamma - d\sin\gamma - R - d)}{6d^2(R+d-R\sin\gamma)^2} - \frac{A\tan\gamma [d\sin\gamma + R\sin\gamma + R\cos(2\gamma)]}{6\cos\gamma(d+R-R\sin\gamma)^2}, \quad (19)$$

where R is the radius of the spherical cap, γ is the angle of the cone, and A is a parameter that defines the conic section and cap. This predicts the z-component of the force, since it is this component that will cause the cantilever to bend.

This result can be compared to Equation (18) by considering the limit where γ approaches zero (no conic section) and the tip is close to the sample, so that $\frac{d}{R}$ also approaches zero. In this case,

$$\lim_{\gamma \rightarrow 0, \frac{d}{R} \rightarrow 0} F_z = -\frac{AR}{6d^2}. \quad (20)$$

This is the same as in Equation (18), with $= \frac{\pi^2 q^2 \lambda}{2}$.

While the sphere-plane model can be used for initial calculations, this more complex model will be useful for determining the distance between the tip and the sample.

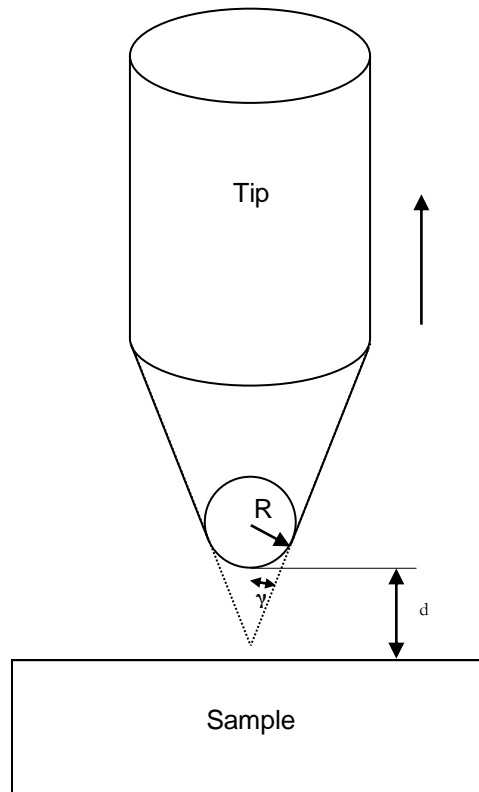


Figure 5. Geometric model of the tip and sample. The sample is modeled as a infinite plane. The tip is modeled as a combination of cylinder, conic section, and spherical cap. This model provides a more accurate basis for calculating the tip-sample forces.

2.3.2 Lateral Forces

The cantilever can be modeled as a lever of length L , width w and height h , as shown in Figure 6. The lateral force on the cantilever with tip length t and shear modulus G is proportional to the lateral displacement in the y direction, Δy , by a proportionality constant called the lateral restoring constant (with units of N m^{-1}) [11]

$$k_{c,lat} = \frac{wh^3G}{3Lt^2}. \quad (21)$$

This gives the relationship:

$$F_{lat} = k_{c,lat}\Delta y = \frac{wh^3G}{3Lt^2} \Delta y. \quad (22)$$

The angle θ by which the tip is rotated about the x axis is given by

$$\sin\theta \approx \theta = \frac{\Delta y}{t} \quad (23)$$

as can be seen in Figure 7. The small angle approximation has been used, since the tip height t is much greater than the deflection Δy .

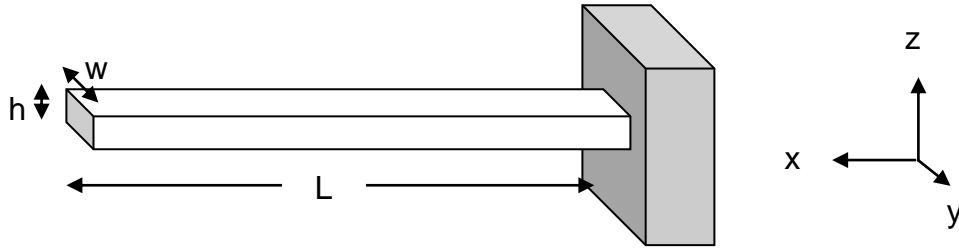


Figure 6. The cantilever is modeled as a rod of length L , height h and width w . The end is free to move up and down (in the z -direction) or laterally (in the y -direction)

Thus the lateral force on the tip, in terms of the angle of deflection is

$$F_{lat} = \frac{wh^3G\theta}{3Lt}. \quad (24)$$

It is important to note that this lateral force is most significant when the AFM is operating in a mode where the tip is in nearly constant contact with the surface. If the tip and sample are oscillating with respect to one another, this lateral force is released each time the tip and sample are separated [12].

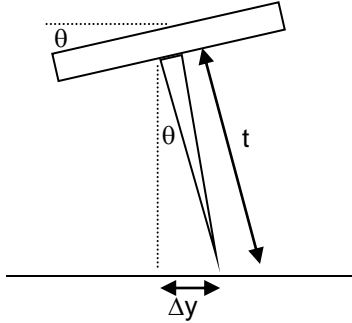


Figure 7. Lateral forces on the tip cause the tip to rotate by some angle θ , which can be measured using a laser deflection system. This allows the lateral force on the tip to be measured.

2.3.3 Capillary Forces

Whenever an AFM is operated in ambient air, a contamination layer must be considered. This layer is typically between 1 and 50 nm [13]. Depending on the mode of operation, it is really the contamination layer that is being imaged. Although this layer may coat the sample fairly consistently, thus giving a reasonable image of the surface underneath, it will still serve to make the image 'blurry'. While different imaging modes lessen this problem, another alternative is to operate the AFM in UHV.

It is also important to note that, for modes which operate inside the contamination layer, the Van der Waals force may in fact be repulsive, rather than attractive, depending on the materials of the tip and sample [9].

2.4 Modes of Operation

There are two main modes of operation for the typical atomic force microscope: Contact Mode and Vibrating Mode. Each mode can be used to investigate specific properties of the sample.

2.4.1 Contact Mode

In this mode, the tip is dragged across the sample. The force on the cantilever tip is kept constant through means of a feedback loop, as shown in Figure 8. This feedback loop is used to record the topography of the sample.

2.4.2 Vibrating Mode

In this mode, the cantilever tip (and/or the sample) is set oscillating at its resonant frequency. As the sample is brought close to the tip, forces between the sample and the tip cause the frequency of the oscillations to change. The sample is then moved using the feedback loop, as shown in Figure 8, so that the frequency of the oscillations remains constant. The movement of the sample corresponds to the topography of the sample.

Depending on the frequency and amplitude of oscillations, the vibrating mode can be further subdivided into three more modes, each of which provides different information about the sample. The modes can be classified by their penetration into the contamination layer on the surface of the sample. The first of these modes operates in the region above the contamination layer. Even when high vibration frequency and a stiff tip are used, the image will be obscured slightly by the

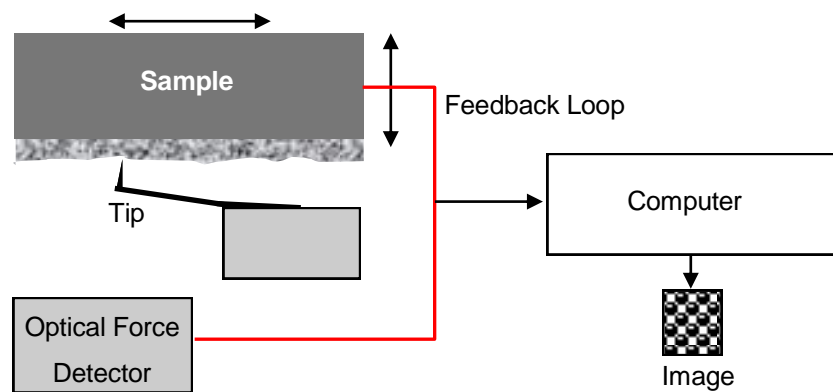


Figure 8. Schematic of an AFM. The tip interacts with the sample in either of the two modes. The force sensor measures the force on the cantilever by measuring a change in the bend of the cantilever or a change in the oscillations. The feedback loop moves the sample so that this force is constant. The computer uses the output of the feedback loop to create the image.

contamination layer. The second mode, called the “tapping” mode, operates in and out of the contamination layer. The fine tuning to do this is less than for the other modes, but there is more potential to damage the tip or the sample since the tip has relatively high energy as it interacts with the sample. The third is called the “near contact” mode, and operates inside the contamination layer. A small amplitude of oscillation must be used for this mode in order to keep the tip inside the layer.

2.5 Tip Geometry Effects

The accuracy of images obtained using the AFM depends directly on the geometry of the tip that probes the surface. Consider the two tip shapes shown in Figure 9 and the resulting scans. It is clear that the narrower tip does a better job of imaging the narrow grooves in the surface of the sample. It can also be seen that neither of the tips accurately represents the surface of the sample. The main difference between (a) and (b) is the width of the tip. For any tip that comes to a point, the image of the sample will be affected by angle which defines the cone-shaped point, as seen Figure 10.

Figure 11 compares tips of entirely different shape. Both tips are able to image the height and depth of the surface features. Tip (b) however, has a beveled edge that allows further detail to be recorded. The first scan (a), extrapolated into a scan across the entire surface of the sample, would result in an image that is sometimes called 2.5-dimensional [14]. Scan (b) would create a 3-dimensional image of

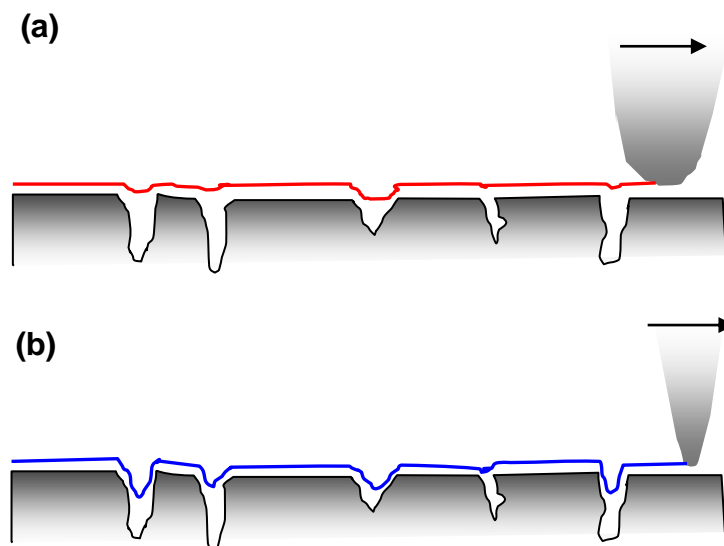


Figure 9. Two different tip shapes create different images of a grooved sample. (a) The large rounded tip does not measure the depth of the grooves and almost entirely misses some features. (b) The narrower tip does a better job of imaging, though some detail is still lost.

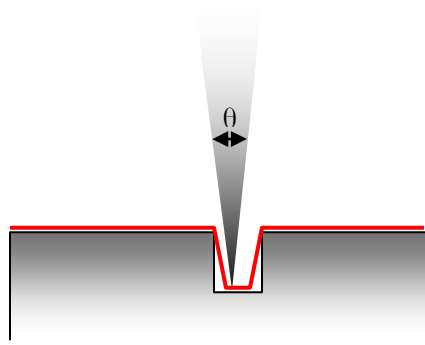


Figure 10. The image of the surface is directly related to the angle which defines the pointed tip.

the sample. Scan (b) would also require more a complex scanning mechanism, including sensing of forces in all different directions (not just up and down) and motion that repeats scanning the same location. For most purposes, the first image would be sufficient, but it is important to understand the inherent image distortions due to tip shape and to consider possible ways of avoiding them. In this case, the problems inherent to the solution seem worse than the original distortions.

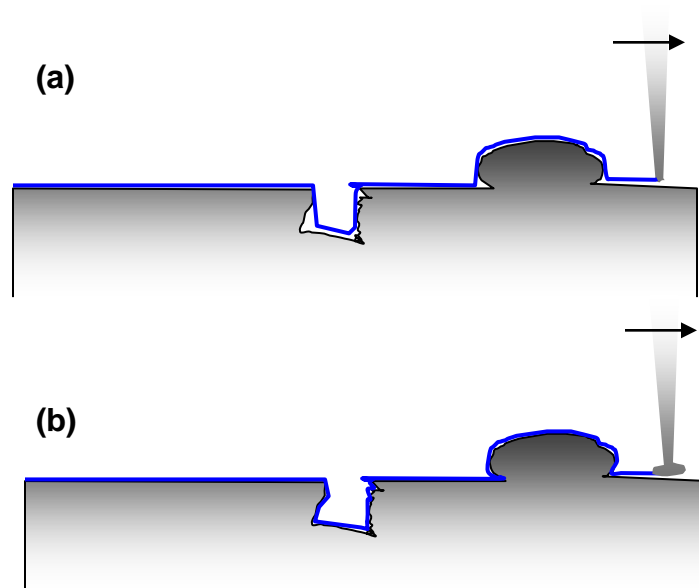


Figure 11. Further changes in tip geometry affect the image. (a) A narrow triangular shaped tip accurately represents the height and depth of surface features, but misses undercut

features. (b) A tip with a beveled end allows for a more 3-D imaging of the sample to take place, but requires significant modifications to the AFM design.

2.6 Tip Characterization

Since tip geometry has such a marked effect on the accuracy of the image, ways have been developed to image the geometry of AFM tips. These include imaging through use of another type of microscopy, such as transmission electron microscopy (TEM) or scanning electron microscopy (SEM). These methods provide two-dimensional images of the tip.

The tip can also be characterized by using the image it produces when imaging a surface with known features, as described by Villarrubia [15]. Sharp features on the surface create an inverted image of the tip. The precision of this method is limited by the sharpness of the features on the surface. It should also be noted that this method creates a 3-D image of the tip only where the tip has touched the characterization surface. Thus undercut features on the tip will not be accounted for. For careful work, this characterization is done both before and after imaging.

Villarrubia [15] also discusses the method of blind tip characterization. This method makes use of sharp features on an unknown sample to image the tip. An iterative technique is used to determine the shape of the tip which works with the scanned image. The results of this blind characterization method were compared with SEM profile images of the same tips, with remarkably close correspondence. This self-consistent method is useful since it is performed in situ and has a reduced risk of damage to the tip. One major limitation is that the resolution of the image obtained after correction by tip shape is limited by the sharpest features on the surface. Thus resolution of these sharp features will lie within the error of the obtained image. This technique is more useful when resolution in the mid range, between the sharpest features and the flattest parts, is desired.

Theoretical methods are also being developed for blind estimation of tips which have an undercut shape [14], as shown in Figure 11. This method utilizes a form of mathematical modeling called dixel representation. It remains to be seen if the methods are as feasible and effective as they claim to be.

For the current stage of this project, it will be clear from images of samples with known topography whether or not the tip has a sharp point. More detailed studies in the future will likely provide incentive to use more complex methods of tip characterization.

2.7 Measurement of the Oscillations of the Cantilever

The first AFM used a STM tip to measure the oscillations of the cantilever tip and to drive the feedback loop, as described in above. The STM tip, however, exerted a force on the cantilever on the order of 10^{-7} N [16]. Since then, an optical method that exerts almost no force on the cantilever has been used. Another advantage to the optical approach is that it can more easily detect larger amplitude changes than the STM tip scheme [17].

The standard optical method is to determine the oscillations of the cantilever through use of a laser and a quadrant detector. The back of the cantilever tip is often coated with aluminum to make it reflective [18]. A laser is then shone on the tip and reflected into the detector, as shown in Figure 12. As the cantilever oscillates, the laser is reflected into different parts of the detector. This is the method that is used in the AFM for this paper.

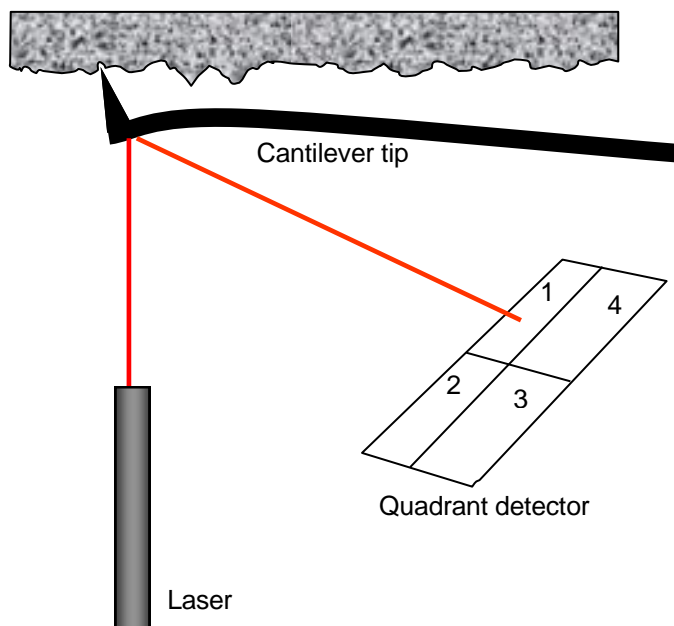


Figure 12. Diagram showing how the laser is reflected off the cantilever tip and into the quadrant detector. In the instance shown, movement into cell 2 would show a change in

topography and movement into cell 4 would show that the tip is experiencing torsion due to frictional forces.

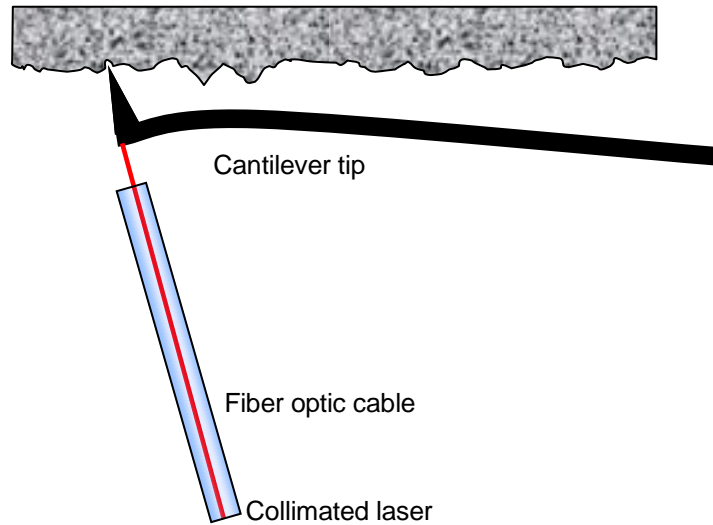


Figure 13. Measurement of the oscillations of the cantilever tip through interferometric methods. The light is reflected off the tip back into the fiber optic, and the light interferes destructively or constructively depending on the width of the gap between the tip and the cable.

Another type of optical method is through use of an interferometric detection system, as outlined by Stark *et. al.* [19]. Rather than measuring the change in angle of the cantilever, this method measures a displacement of the tip by a certain distance. A fiber optic cable is used to focus the laser light on the cantilever, perpendicular to the lever, as shown in Figure 13. This light reflects back into the cable, interfering constructively or destructively depending on the distance between the detector and the cantilever tip. A photodiode is used to detect the interference signal. This method has been used for imaging low temperatures (mK range) since very little power is delivered to the tip [20], and for magnetic force microscopy [21], with the hopes that it will have less thermal drift than other optical detection methods. It also features the advantage of being compact. Since the laser system has not yet been fully implemented in the construction of this AFM, it is useful to consider the advantages of this optical measurement system.

2.8 Sources of Noise

Since it was the ability to minimize sources of noise which led to the development of the STM and subsequently the AFM, it is important to consider possible sources of noise. The primary source of noise which must be avoided is external vibrational noise. These vibrations, coming from the heating system in the building or a nearby road or any other similar and uncontrollable source, can make imaging impossible. For this reason, the isolation system is an important component to the microscope.

There are also sources of noise from the system itself. Sarid [22] identifies three primary components to the AFM system which contribute to noise: the cantilever, the laser deflection detection system, and the piezos which drive the oscillations. Since the laser system is not yet in place, analysis of this noise will be considered in a later study. Cantilever noise and piezo error are discussed in the following sections.

2.9 Thermal Effects

2.9.1 Thermal Noise of the Cantilever

Thermal effects give rise to one of the primary sources of noise in the AFM, especially on the cantilever. Butt and Jaschke have calculated the thermal noise for the cantilever of the AFM [23]. The cantilever can be modeled as a rectangular prism of length L , width w and height h , as shown in Figure 6. The spring constant K is given by

$$K = \frac{Ewh^3}{4L^3} \quad (25)$$

where E is the modulus of elasticity. According to the equipartition theorem, the mean energy of the cantilever must be given by kT , with k being Boltzmann's constant. Thus

$$kT = K\langle z^2 \rangle \quad (26)$$

So that

$$\sqrt{\langle z^2 \rangle} = \sqrt{\frac{kT}{K}} \quad (27)$$

and $\langle z^2 \rangle$ is the mean square deflection due to thermal noise. For measurement using optical deflection rather than an interferometer, as discussed on above, the calculation of thermal noise is rather complex. The optical deflection system, as discussed, measures the change in angle of the cantilever, and not simply the displacement along one axis. With this consideration in mind, the thermal noise for a cantilever tip fixed only at one end was found to be [23]

$$\sqrt{\langle z^{*2} \rangle} = \sqrt{\frac{4kT}{3K}} \quad (28)$$

The asterisk indicates that the virtual height z^* , as measured using the optical lever method, is being considered.

If the cantilever is fixed at both end, for example when it is in contact with a hard sample, this noise is found to be [23]

$$\sqrt{\langle z^{*2} \rangle} = \sqrt{\frac{kT}{3K}} \quad (29)$$

During measurements with an AFM, the situation will likely be somewhere between these two, depending on the mode of operation and on the hardness or softness of the sample compared to the tip.

2.9.2 Thermal Expansion of different materials

Different solid materials have different thermal expansion coefficients. As these materials cool down or heat up, this can lead to additional shifts in the measurements. Dai *et. al.* have reported change in the alignment of the laser, reporting that this is most likely due to the differing coefficient of expansion of the reflective gold plating on the cantilever from the expansion of the cantilever itself [24]. This must be taken into account when analyzing the images taken with the AFM.

Since the aim of this project is to build a variable temperature AFM, effects due to differing coefficients of expansion have been carefully considered in the design of the microscope, as will be discussed in section 3.2

2.9.3 *Thermal Effects on the Cantilever Due to the Laser*

Another possible source error in measurements taken using the cantilever and laser setup is due to the effects of the laser on the cantilever. A study by Allegrini *et. al.* [25] was conducted in which the thermal effects as well as the radiation pressure of the laser light were studied for different cantilever constructions. It was found that, while there were indeed some radiation pressure effects, they were minimal. More importantly, the thermal effects were found produce a significant amount of error. The worst cantilever design was found to be the design in which the back of the cantilever had a reflective gold coating on it. These gold-coated cantilevers were found to be deflected more than 1 μm by laser heating. This is a significant amount, and must be considered when choosing the tip design to be used.

2.10 Piezoelectric crystals

2.10.1 *The Piezoelectric Effect*

The piezoelectric effect is a property exhibited by certain crystalline materials in which they produce charge when compressed. In 1881 G. Lippman [26] proposed the converse: if a potential difference is applied to these materials, they will change shape. This ability to convert electric potential into kinetic energy is critical to the operation of the AFM.

Consider the cylinder shown in Figure 14 made of a piezoelectric material. There are 5 electrodes on the cylinder, as denoted by the numbers. Let electrode 1 be at ground. If the potential of electrodes 2-5 is increased, the piezo ceramic between the plates will be compressed horizontally, causing the ceramic to expand in the direction perpendicular to the field. This will cause the cylinder will increase in height. If the potential of electrode 2 is increased while the potential of electrode 4 is decreased, the far side of the cylinder will be compressed to become thinner and thus taller, while the front will become thicker and shorter, causing the cylinder to bend forward. Combinations of these two types of motion allow a full range of motion in any direction, allowing complete control of sample or tip through electric signals.

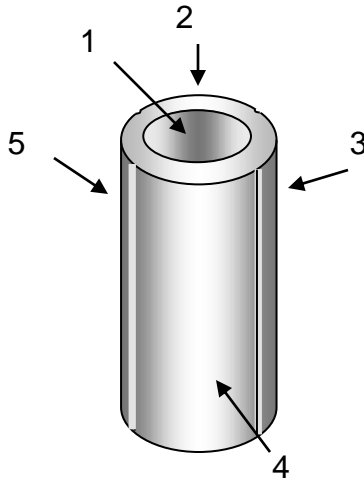


Figure 14. Diagram of a cylindrical piezoelectric ceramic. The numbers denote five electrodes which have been attached to the ceramic, with electrode 1 on the inside and electrodes 2-5 on the outside. If a voltage is applied to these electrodes, the cylinder will change shape. If the potential is increased between two electrodes, the ceramic will compress in that direction and expand in the direction where there are no electrodes.

2.10.2 Sources of Error

While the piezoelectric ceramics provide a means of positioning the sample and tip with incredible precision, there are still errors inherent in their usage. Two of the primary sources of error arise from the effects of hysteresis and creep.

Hysteresis arises from the nonlinearity of the ceramics. The amount by which the dimensions of the material change is not directly proportional to the voltage applied. The ceramic tends to maintain its original shape so that the dimensional change is initially slower than the ramp speed [27]. This effect must be corrected for when using piezoelectric ceramics for positioning.

Creep arises when, after a sudden voltage change to a piezoelectric material, the dimensions of the material slowly continue to change, even while the voltage remains constant.

Many methods have been employed to correct for these sources of error. Most of them include a separate detector which monitors the piezo. These techniques include feedback based, feedforward

control, or a combination of both [28]. Although not a part of the current design, such a monitor would be a useful tool for eliminating a large source of noise.

2.10.3 “Stick-Slip” Theory of Approach

One useful application of piezos is in a method of positioning using a “stick-slip” process. For this method, a piezo tube like the one shown in Figure 14 supports an object on top and has a sapphire ball attached to the other end. It rests on a smooth surface. The piezo tube begins in the upright position, as shown in Figure 15 (a). A voltage is then applied to the piezo so that it bends to the shape shown in Figure 15 (b). This could be achieved, for example, by gradually applying a large positive voltage to electrode 3 in Figure 14 and a large negative voltage to electrode 5. The force of static friction between the sapphire ball and the surface keeps the end from moving. The voltage is then suddenly reversed so that the piezo returns to its original shape, as shown in Figure 15 (c). This happens so quickly that the force of friction is overcome and the sapphire ball moves along the surface. This can be repeated as often as desired, moving the whole device to the right. The voltage pattern for one electrode required to achieve this resembles a saw-tooth pattern on a voltage versus time plot, as shown in Figure 15 (d). The voltage on the other electrode is the opposite. Depending on the voltages applied, the device can be moved in any direction in the horizontal plane.

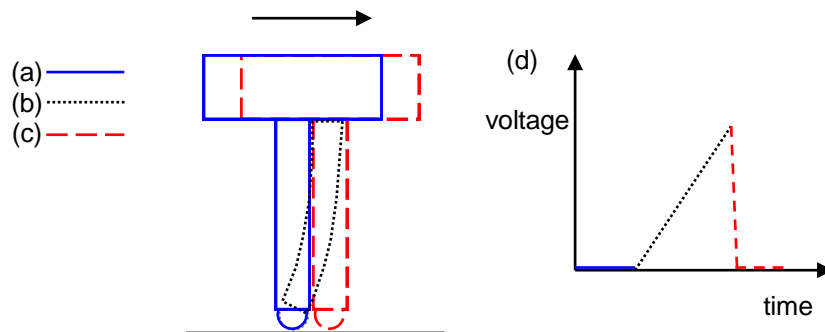


Figure 15. The three steps of stick-slip motion are shown. A piezo tube supports an object at one end and has a sapphire ball attached to the other end, which rests on a smooth surface. (a) The piezo tube is upright. (b) Voltages are applied to bend the tube. Friction holds the end against the surface. (c) The voltages are suddenly reversed, causing the tube to snap back into shape, exerting a force greater than the force of the static friction between the sapphire ball and the surface. The whole apparatus has now moved to the right.

Chapter 3

A VARIABLE TEMPERATURE AFM

3.1 Model

Dai *et. al.* [24] reported construction of a variable temperature ultra high vacuum (UHV) AFM in 1995. Their microscope made use of a liquid nitrogen-cooled reservoir for cooling the sample and various methods for heating the sample. While images were taken at different temperatures, it seems that some trouble was experienced with thermal drift and that only very slow temperature change provided the stability necessary to make good AFM images. We have used their design as a starting place and made significant modifications which we hope will enable imaging during more rapid temperature changes.

3.2 Overall Design

The overall design of the variable temperature AFM is shown in Figure 16. The design uses some of the elements of the AFM built by Dai *et. al.* [24], including a “Johnny walker” for movement and a laser system for detection of the sample. In this design, however, the sample and cantilever are inverted so that the sample faces downward onto the tip. This change was made so as to more easily separate the scanning apparatus, which needs to have a high resonant frequency and should be isolated from the system, from the detection apparatus. Care has been taken to ensure that the materials used in construction are grouped in symmetric layers so that thermal expansion and contraction will not seriously misalign the microscope.

3.3 Damping System

The damping system consists of two main parts which work together to damp oscillations. First of all, the microscope is mounted onto a heavy base that hangs from four springs, as shown in Figure 17. The springs are securely attached to a support, which is attached to an optical table. The base has a mass of 2.2 kg so that the spring system has a low resonant frequency of about 0.9Hz.

To keep the whole system from oscillating, four grade N42 neodymium magnets with a surface field of 3250 Gauss (0.325 T) are placed in slots in the metal base. If the base moves up and down, it moves through differing regions of the non-homogeneous magnetic field produced by the magnets.

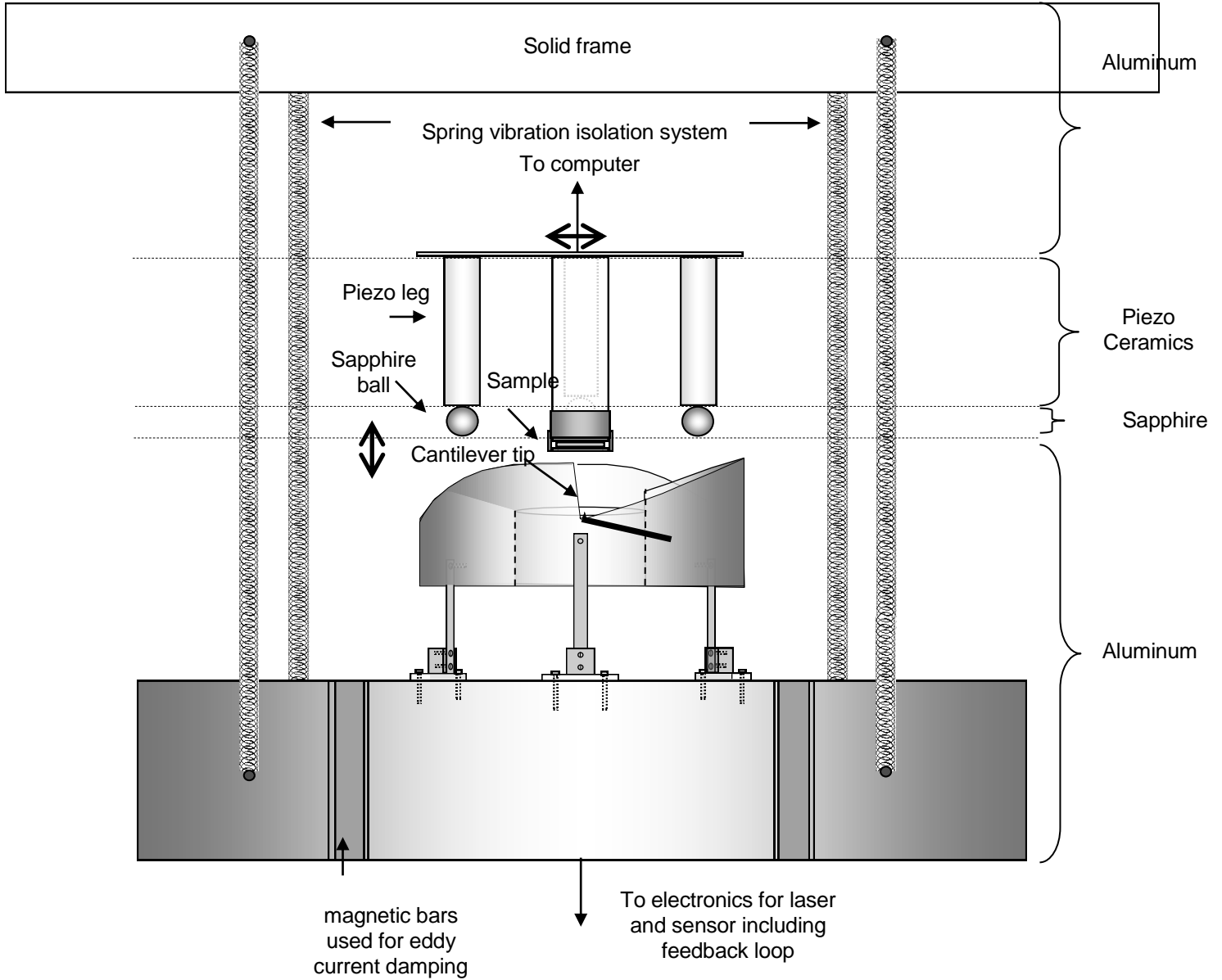


Figure 16. Schematic diagram of the AFM (not to scale). The “Johnny Walker” sample mount can be seen, with the corresponding ramp. The isolation system consists of two parts: the system is hung from springs and slots in the base hold magnets which provide

eddy current damping. The materials used are carefully divided into sections so that heating and cooling will cause everything to expand and contract together.

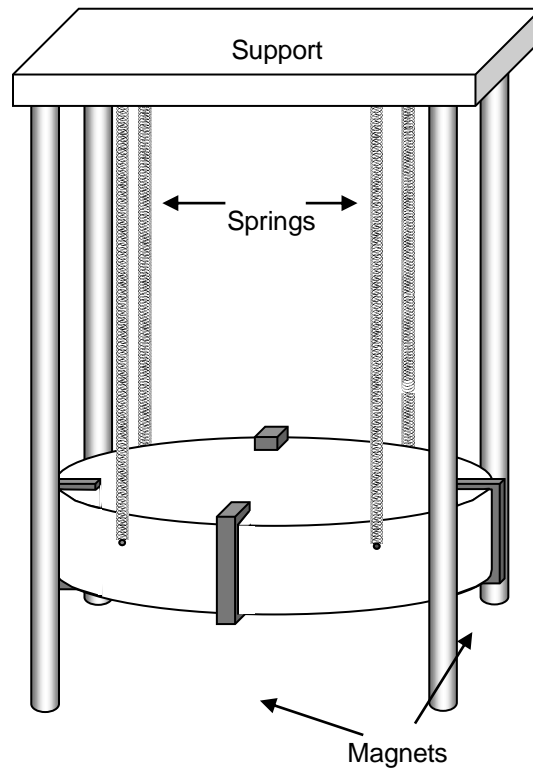


Figure 17. A diagram of the damping system is shown. The base for the microscope hangs from a support structure by four springs. Four magnets are held in place by clamps (clamps not shown) The magnets induce eddy currents in the metal base which create magnetic fields which oppose up and down motion, thus damping oscillations of the springs.

According to Lenz's law, this will induce currents in the metal in the direction that will create a magnetic field which opposes the change in the magnetic flux. This results in a force opposing the motion; thus the oscillations are damped.

3.4 Movement of the Sample

3.4.1 Positioning of the Sample

As shown in Figure 16, the sample is mounted on a tripod formed by three piezo tubes. This setup, called a "Johnny Walker", is what allows the sample to be moved up and down. Using the stick-slip

method of approach described in Section 2.10.3, the piezo tubes act as legs which walk up or down the ramp. This ramp is divided into three portions, each of which has a 10° slope both tangent to and perpendicular to the curve. A piezo leg sits on each portion of the ramp. The saw-tooth voltage pattern that drives the three “legs” is timed so that all three tubes move at once. This will be described in greater detail in Section 3.8.2.2.

In order to ensure that the sample and tip are not damaged by having them come in contact, the laser and sensor system is utilized. Before each “step”, the computer checks to see if the sensor reads of change. This is done by changing the potential of the inner electrode so as to gradually move the sample down and back up. In order to move the sample up, a negative voltage is applied to the inner electrodes on each of the piezo tubes, causing them to lengthen. A positive voltage will shorten the tubes and move the sample down. If the laser system detects that the tip has come close to the sample during one of these cycles, the slip and stick motion will not proceed any further.

Further fine-tuning of the position can be done by applying potential which bends the piezos in specific directions, without actually moving the ends of them through means of slip and stick motion. This is accomplished by applying a potential which bends the piezos and exerts a force which is lower than the force of static friction. This allows the exact location of the scan on the surface of the sample to be selected. The applied voltage for this motion is the same as for the scanning of the sample, described below.

3.4.2 Scanning of the Sample

Once the sample is positioned so that the area to be scanned is close to the tip, a new mechanism must be used to scan the sample. There are three components to making a three-dimensional scan: scanning up and down, rastering in the x (or y) direction, and slowly scanning along the y (or x) direction. The up and down motion is controlled by the feedback loop driven by the sensor, as described in Section 2.4. The motion up or down is achieved by applying lower or higher potentials, respectively, to the inner electrodes on each piezo.

The rastering is achieved by driving the legs with a triangle voltage, as shown in Figure 18. As an increasing voltage is applied to one of the electrodes on the piezo (the first part of the triangle

function), it begins to bend to the left. As this voltage is decreased, it bends back and then begins to bend to the right as the applied voltage becomes negative (with respect to the center, a floating ground). The opposite function is applied to the electrode on the other side of the tube. This function is repeated, causing the sample holder to scan back and forth. Another triangle function with a lower frequency is applied to the electrodes which face perpendicular, causing the scan to move slowly across the sample.

As the piezo tube bends back and forth, the sample mount height will change slightly. However, since the radius of curvature of the piezos is so large compared to the size of the scan, this effect will only cause minor distortions that can be taken into account when calibrating and analyzing the scans but need not be accounted for in the physical design.

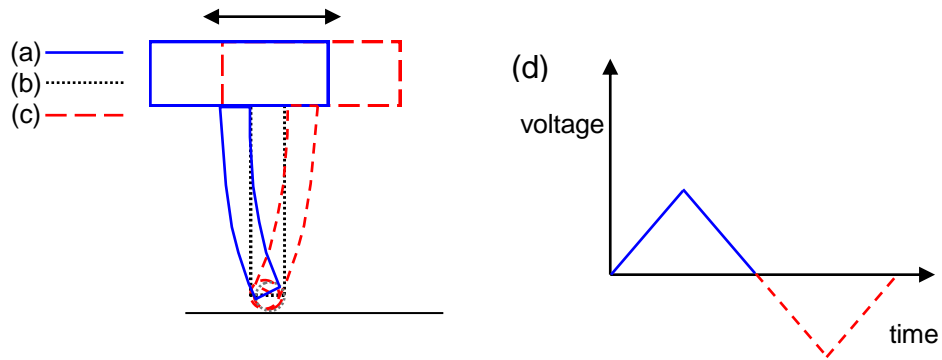


Figure 18. (a)-(c): Voltages applied to the piezo tubes in a saw-tooth pattern cause the sample to scan back and forth. (d): The saw-tooth shown would be applied to one electrode. The negative of this pattern would simultaneously be applied to the electrode on the opposite side of the cylinder.

3.5 Oscillations of the Cantilever

The oscillations of the cantilever are driven by a small piece of piezo ceramic on which the cantilever rests, as seen in Figure 19. One side of this ceramic is tied to ground and an oscillating potential is applied to the other side.

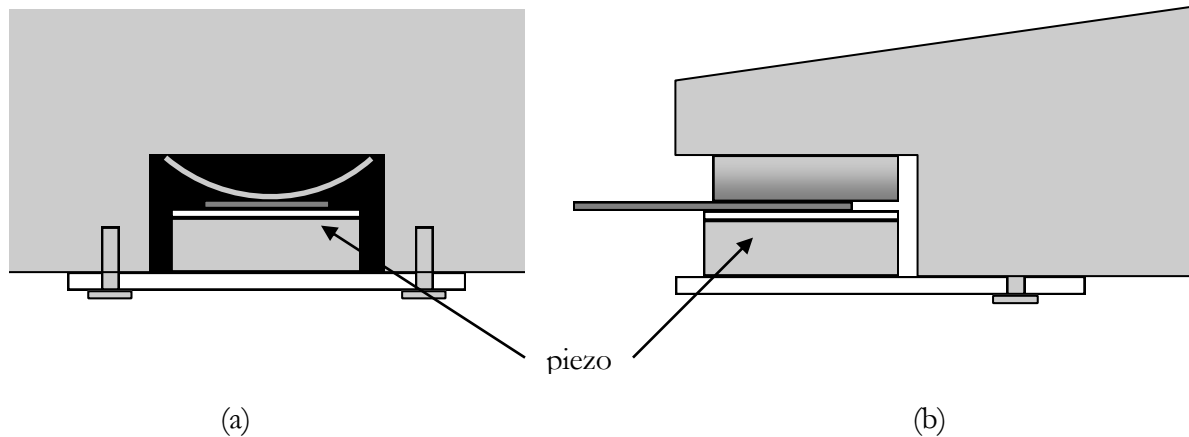


Figure 19. Design of the cantilever driver. (a) Front view, as seen from the center of the ramp. (b) Side cut-away view. The light gray portions are aluminum and the white portions are ceramic. The cantilever holder is dark gray. The piezo sits below the holder, as shown. A curved piece of aluminum keeps the holder in place and connects the top of it to the rest of the ramp, which is tied to ground.

3.6 Heating and Cooling

As discussed earlier, one of the goals of this project is to enable imaging of samples as they undergo temperature change. Included in the design of this microscope is a means of heating and cooling the sample. Dai *et. al.* [24] use a cold finger which uses liquid nitrogen to cool their sample to below 90K and resistive heating to heat up their sample. This method will also be adopted for this project, although placement of the heating and cooling elements will differ. As can be seen in Figure 16, the sample holder and ramp on which the tip is mounted are isolated from the base by ceramic plates. This isolation will be useful for fine-tuning the rate of temperature change of the sample. Further work is yet to be done on optimizing the design for the heating and cooling system.

3.7 LabVIEW Program

LabVIEW 8.2 (student edition) was used to create the program that runs the microscope. This program drives the piezos, reads the input from the laser detector, and stores the scan to create maps of the surface. While there is one overall program which provides a convenient user interface, the program as a whole is divided down in to smaller sub-programs which perform specific tasks. These sub programs include a program for “walking” the sample mount up and down the ramp (the

approach program), a program for manually moving around on the sample surface to choose the scanning area, a program for scanning, and a program for making the maps.

3.7.1 The Approach Sub-Program

The approach sub-program shown in Figure 20. Steps which are circled indicate direct input by the user.

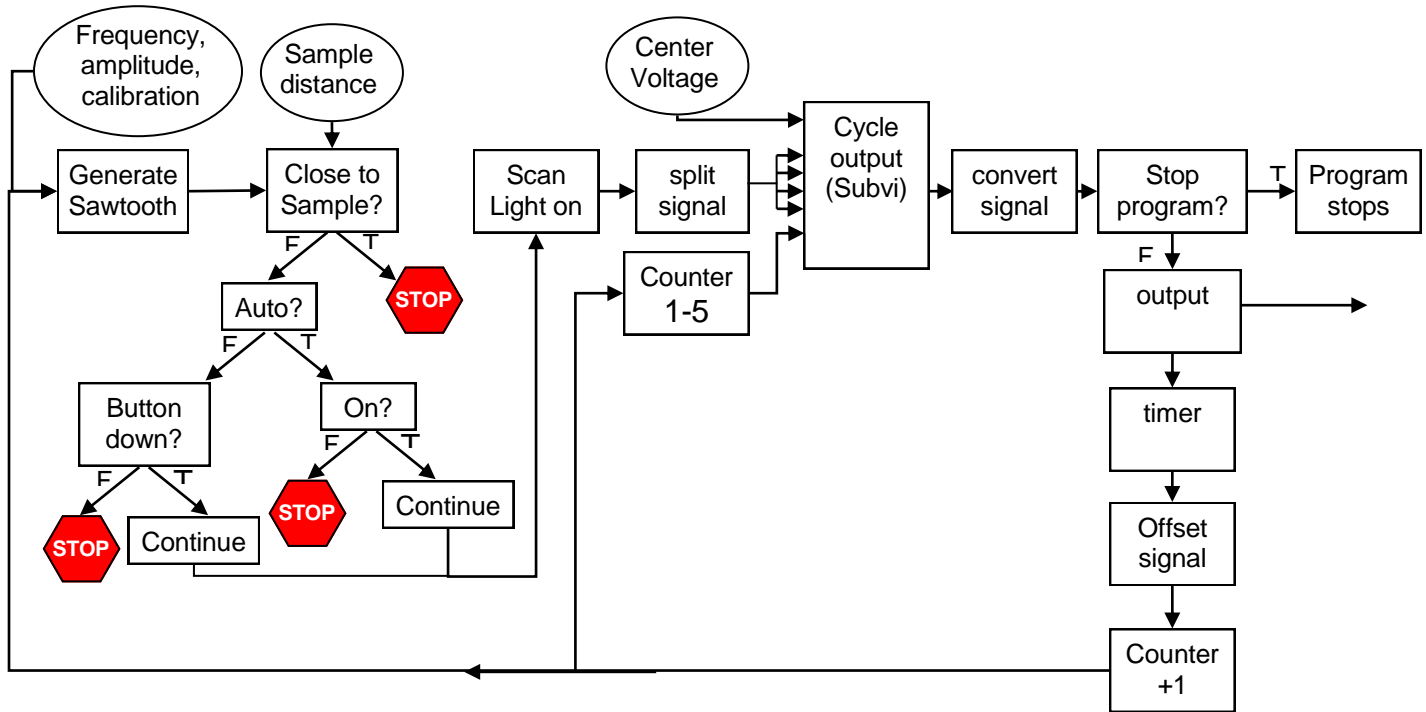


Figure 20. Logic diagram for the “approach” sub-program. Circled items indicate direct user input. A saw-tooth wave function is generated, based on user inputs. The program then executes a series of checks to determine if it a voltage should be output or not. These checks depend largely on the user inputs, but also on the input from the laser, which indicates the tip-sample distance. Once everything is ready for the movement to proceed, a light turns on in the interface, indicating that the sample mount is in motion. The signal is then split and input into a Subvi which cycles through the signals. Then the signal is converted and output to the conversion circuit. The loop continues until the user stops it, each time counting up one and offsetting the signal by a given amount in order to move to the next point on the function. Note that the timing of the loop can be controlled.

First, a saw-tooth function is generated for the slip-stick motion, as described in Section 2.10.3 and in Figure 15. A preview of the shape of this saw-tooth is output to the user and then a check is made to see if the signal should continue to be sent. If not, a voltage of zero is output until the user directs that the scan is ready AND the laser input indicates that the sample is not already at the correct distance from the tip. This signal is then divided into five different signals (four saw-tooth functions and one center “ground” voltage), as discussed in Section 3.8.2.2. However, since only one signal can be output at a time, these signals are put into a subVI (sub- virtual instrument) which cycles through all five signals, outputting the next one each time the loop repeats. Next, the signal is converted into a 12-bit binary array, as appropriate for the electronic circuit, for output to the Signal Conversion Circuit. This effectively takes the first value of the signal array. Thus, when the loop is repeated, the signal is offset by a specified value, effectively taking the next point on that function. This also allows the user to control the step size. All these steps are repeated until the user stops the program. The speed at which this loop executes can be controlled directly, though is most conveniently controlled through the desired frequency input by the user. Three bits are also added which count from 1-5. As the five different functions cycle through the output, these three bits are used by the conversion circuit to specify the electrode to which the signal should be sent. More complete documentation of this program can be found in the Appendix.

3.7.2 The Positioning Sub-Program

Once the sample is close to the tip, it is desirable that the program allow the user to move manually across the surface to select the region to be scanned. This program allows the user to choose the desired step size and then, using either the mouse or the keyboard, to move step by step in any direction.

To enable this kind of control, event structures were utilized. There are multiple “event cases” in any given event structure, each one of which has a trigger and an action, as shown in Figure 21. This type of structure waits to execute until one of the triggers has been set off, and then executes the appropriate action for that case. Only one event case can be executed at a time. This structure is then put inside a while loop, causing the event structure to wait again until the next trigger, and so on, until the stop button is pressed. Keyboard shortcuts have been implemented, so that the microscope

can be driven easily from the keyboard. More detailed information on each of the event cases can be found in Appendix.

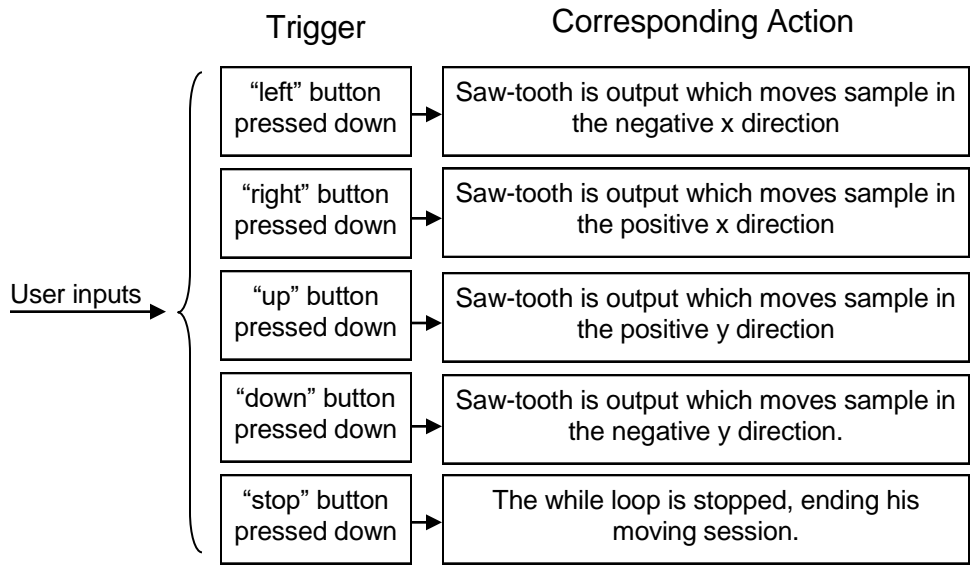


Figure 21. Logic diagram for the main event cases in the Positioning program. Each time one of the triggers is executed by the user through the user interface, the event structure handles the event by executing the corresponding action.

3.7.3 Scanning Sub-Program

The scanning sub-program is one of the most crucial components of the AFM, allowing the surface of the sample to be imaged. As discussed in Section 3.4.2, a triangle wave function, when applied to the electrodes on the sample holder, will cause the holder to move back and forth. This program generates four related triangle waves which enable scanning in both x and y. The functions are coupled so that the second is the inverse of the first and the fourth is the inverse of the third. The related functions are applied to facing electrodes, causing the piezo tubes to bend.

The potential of the electrode in the center of each of the piezos changes according to the input from the laser. This keeps the force on the cantilever at its initially set value. Once the laser system is in place and calibrated, this portion of the program can be fine-tuned so that the user can numerically set the desired tip-sample distance, or tip oscillation amplitude (depending on the mode of operation),

before a scan. The feedback loop will then keep it at that distance. The potential that is output to the center electrodes will also be stored in the memory for use in the mapping program.

The five output signals will then be sent to a cycling sub-program similar to the one in the approach program. This can be easily added once the approach program has been tested.

Once everything has been calibrated, the user can easily set up a scan. The user inputs the dimensions of the scan (in the x and y directions), the number of lines in the scan (resolution), and the desired time of scan. The scan stops after the specified time has elapsed. During scanning, a light indicates that a scan is in progress, and a clock indicates the time elapsed. For further details, see the Appendix.

3.7.4 Future Work on the LabVIEW Program

The program portion of this project is still in the early stages and must be further tested before more extensive development takes place. Aside from the small things already noted, there are other parts of the program that must be developed. The first is a mapping sub-program, which will store the information from the scans and output this information in a useable form. This program should also include corrections for hysteresis and any other distortions inherent in the scan. Another program should also be created to oscillate the cantilever at its resonant frequency. In addition to this, the overall program which both provides an easy user interface and allows for easy switching between modes, must be more carefully developed. Ideally, this program will perform the tasks which are common to all of the programs, such as cycling through the five signals or even receiving the user inputs.

3.8 Electronics

A logic diagram for the overall plan of the electronics is shown in Figure 22. The signals from the computer are input into a circuit which has two primary functions: to convert the signal from digital to analog, and to amplify the signal. The second amplification circuit also has two parts, which direct and divide the amplified signal in different ways, depending on whether the AFM is in approach mode or scanning mode. A switch will be used to change between the two different circuits. The switch will need to have at least 45 pins, since each of the wires going to the electrodes on the three piezos will

need to be re-directed. Another circuit reads the input from the laser detector and inputs it into the computer program.

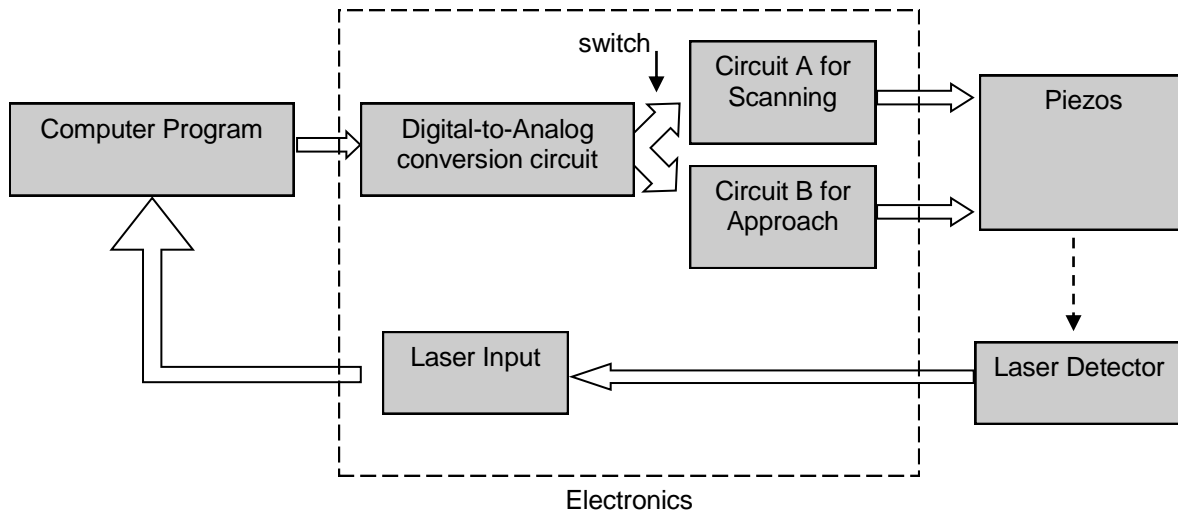


Figure 22. Logic diagram of the function of the electronics in the AFM. The four primary uses for the electronics are for DAC, amplification for both the approach and the scanning modes, and reading of the laser detector input.

3.8.1 Signal Conversion Circuit

The digital output from the computer must first be translated into analog. This circuit is shown in Figure 23. The 15 bit digital output from the computer goes through a NI 6221 (68-pin) board. This signal is then input into two 12 bit DAC7624 digital-to-analog converter (DAC) chips. The signal includes 12 bits which make up the output voltage and three bits which count from 1-5 repetitively, as described on page 36. The 12 bits are used in the input of each chip. The last three bits serve as the address for the output of the analog voltage, specifying which of the four outputs on each chip and which chip is to be used. The outputs A through E are sent directly to the amplification circuits.

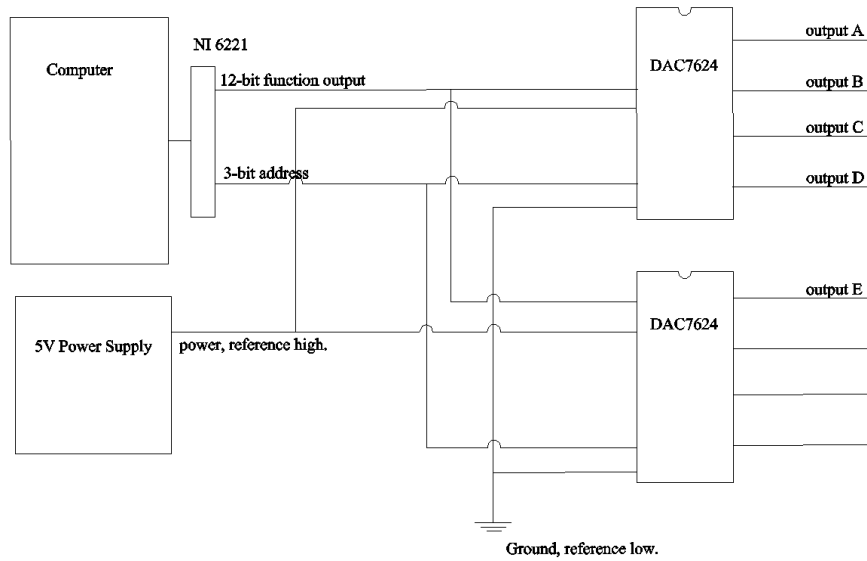


Figure 23. Diagram of DAC circuit. 0-5V digital outputs from the computer program are translated into analog signals by the DAC7624 chips. Reference voltages of 5V and 0V for high and low, respectively, are used so that the outputs A-E range from 0 to 5V.

3.8.2 Amplification Circuits

3.8.2.1 Scanning

The signals from the DAC is amplified using EMCO C20 chips. Each amplifier uses the circuit shown in Figure 24. A RSR HY3002-3 DC power supply set to within the range of 11.5-17 V powers the chip, and the input from the DAC circuit ranges from 0-5 volts.

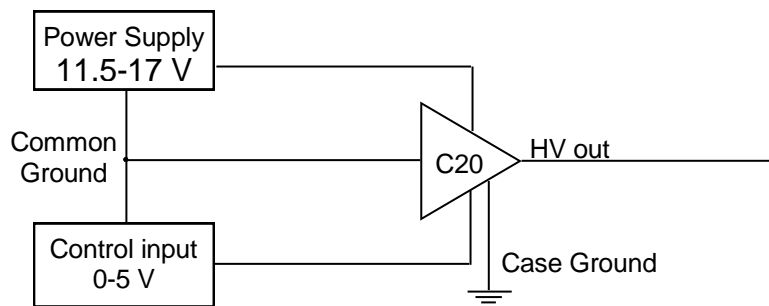


Figure 24. Circuit diagram for EMCO C20 High voltage supply. The power supply and input control are tied to a floating ground with the chip.

Both input and power supply are wired to a common ground with the chip, while the case is tied to a separate ground. This circuit is then repeated for each of the five power supplies, as shown in Figure 25.

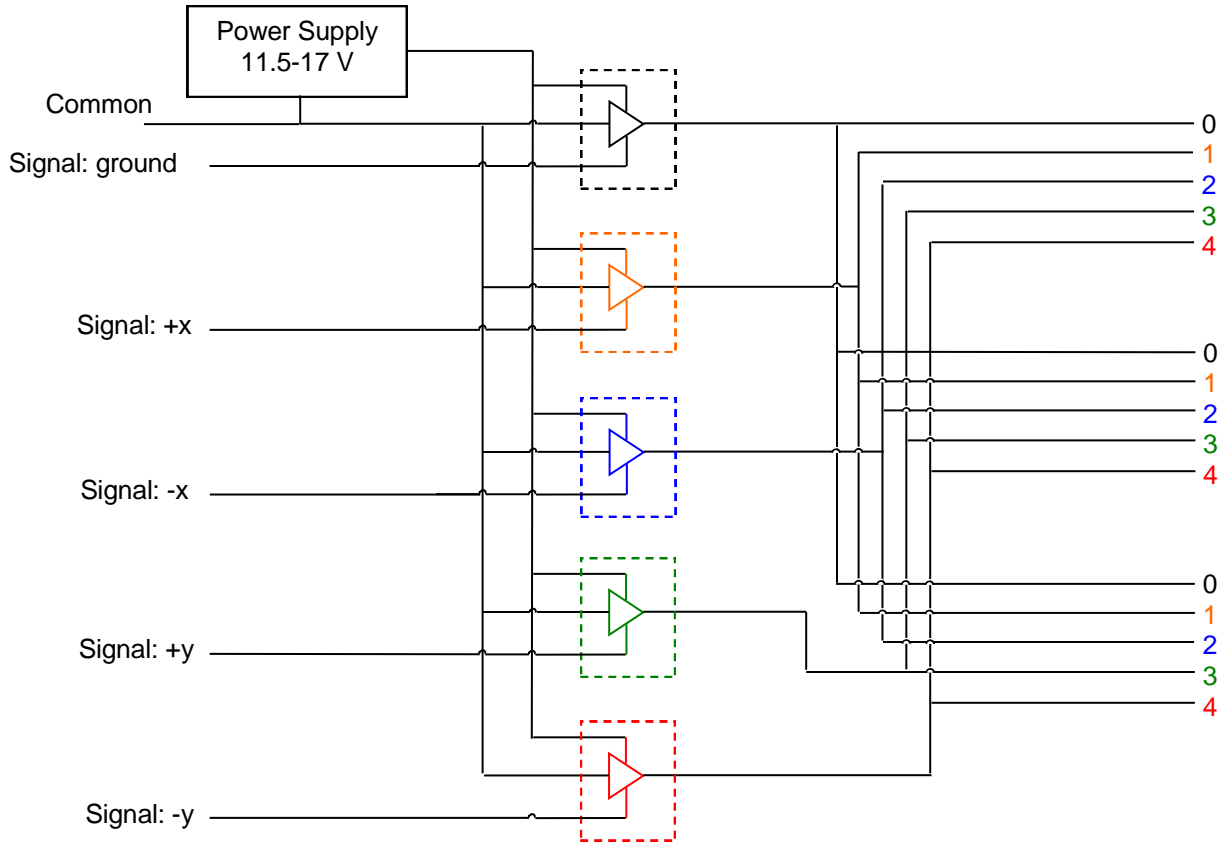


Figure 25. Circuit diagram for scanning. Each input is amplified and sent directly to the corresponding electrode on each of the three piezos (see Figure 26).

Each power supply, as controlled by the computer, corresponds to ground or positive or negative x or y. The amplified signal is wired to the corresponding electrodes on the piezo ceramics, as shown in Figure 26. Electrodes 1, 2, 3, and 4 correspond to the positive x, negative x, positive y and negative y directions, respectively.

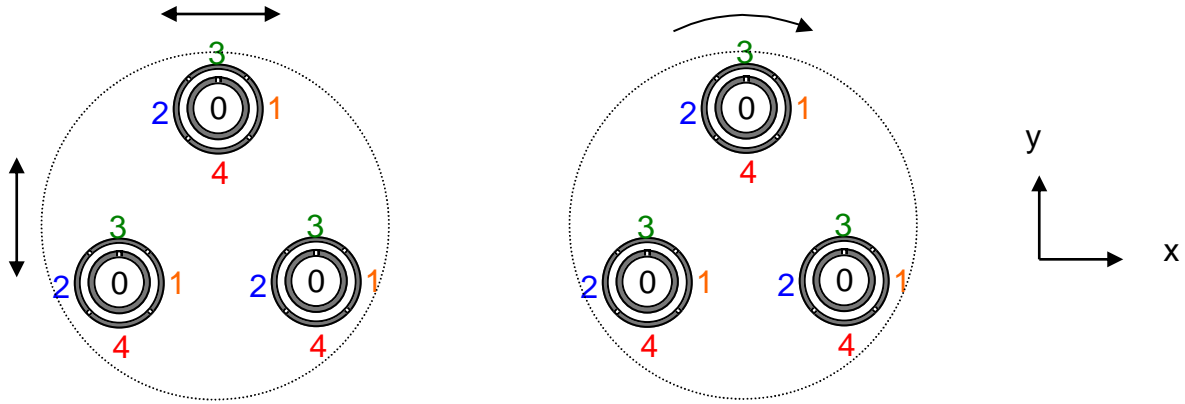


Figure 26. Overhead views of the sample mount, showing the three piezo tubes and their numbered electrodes. The figure on the left shows the direction of motion for scanning, while the figure on the right shows the direction for approaching. For scanning, the electrodes correspond directly to the direction of motion: 1: positive x, 2: negative x, 3: positive y, 4: negative y. For approaching, the voltages must be divided.

3.8.2.2 The Approach

For the approach, the sample mount must rotate in order to walk up or down the ramp. This means that voltage dividers are required to redistribute the potential. Geometry can be used to determine what these voltage divisions should be. An equilateral triangle inscribed in the circle containing the piezos can be drawn, as shown in Figure 27. Motion is tangent to the circle, and can be divided into horizontal and vertical components as shown. If a saw-tooth voltage V_B is applied to the right electrode on the top piezo, then voltages of $\frac{V_B}{2}$ and $\frac{V_B\sqrt{3}}{2}$ must be applied to the left and bottom electrodes, respectively, of the piezo tube on the right. The other electrodes on that piezo will simply be the negative of those potentials, with respect to the ground potential applied to the center of all three piezos. The same reasoning can be used to find the required voltage division for the third piezo.

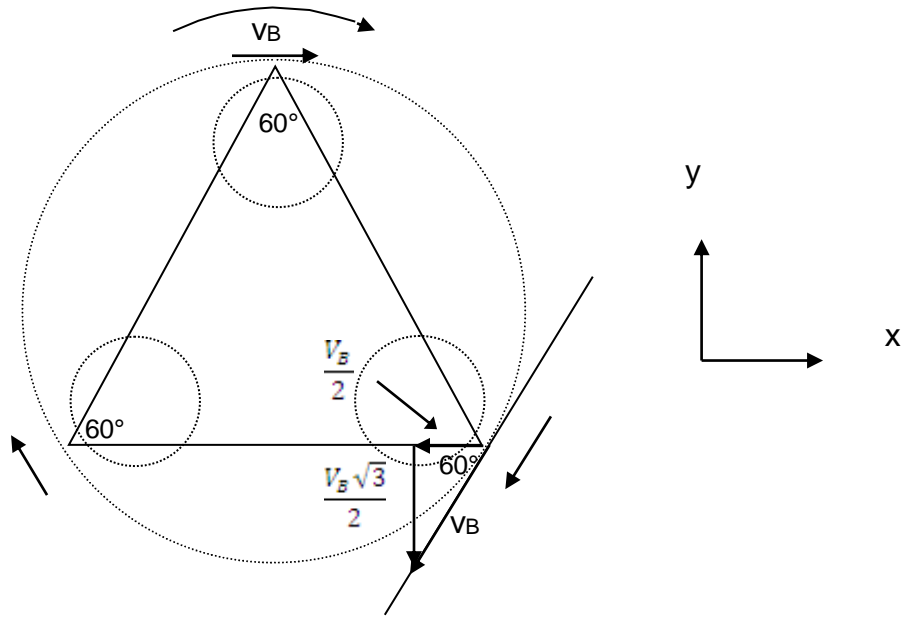


Figure 27. Overhead view of the sample mount, showing the geometry used to calculate the necessary voltage distribution on the horizontal and vertical electrodes of the piezo tubes that are not parallel with the direction of motion.

Thus, if the center electrodes of the tubes are set to some common potential V_A , the distribution of voltage across the rest of the electrodes will be as shown in Figure 28. Most of this can be done in the computer code, but since there are only five power supplies needed for the scanning circuit, it is advantageous to limit the computer output to five different potentials for this circuit as well. The outputs from the computer will be:

1: V_A

2: V_B

3: $V_A - \frac{V_B}{2}$

4: $V_A - \frac{\sqrt{3}V_B}{2}$

5: $V_A - V_B$

The second output can then be split into three outputs using voltage dividers: V_B , $\frac{V_B}{2}$, and $\frac{\sqrt{3}V_B}{2}$. This is shown in the Figure 29. The high voltage outputs are sent to the appropriate electrodes, as described by Figure 28.

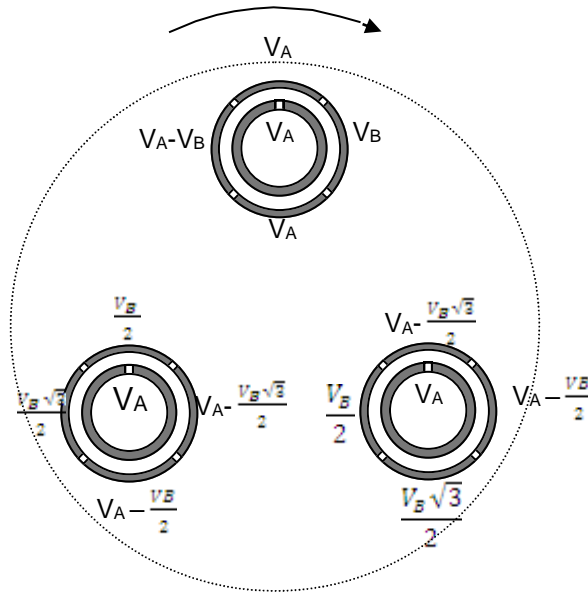


Figure 28. Overhead view of the sample mount, showing the distribution of potential across the electrodes in order for the mount to move in the circular fashion shown.

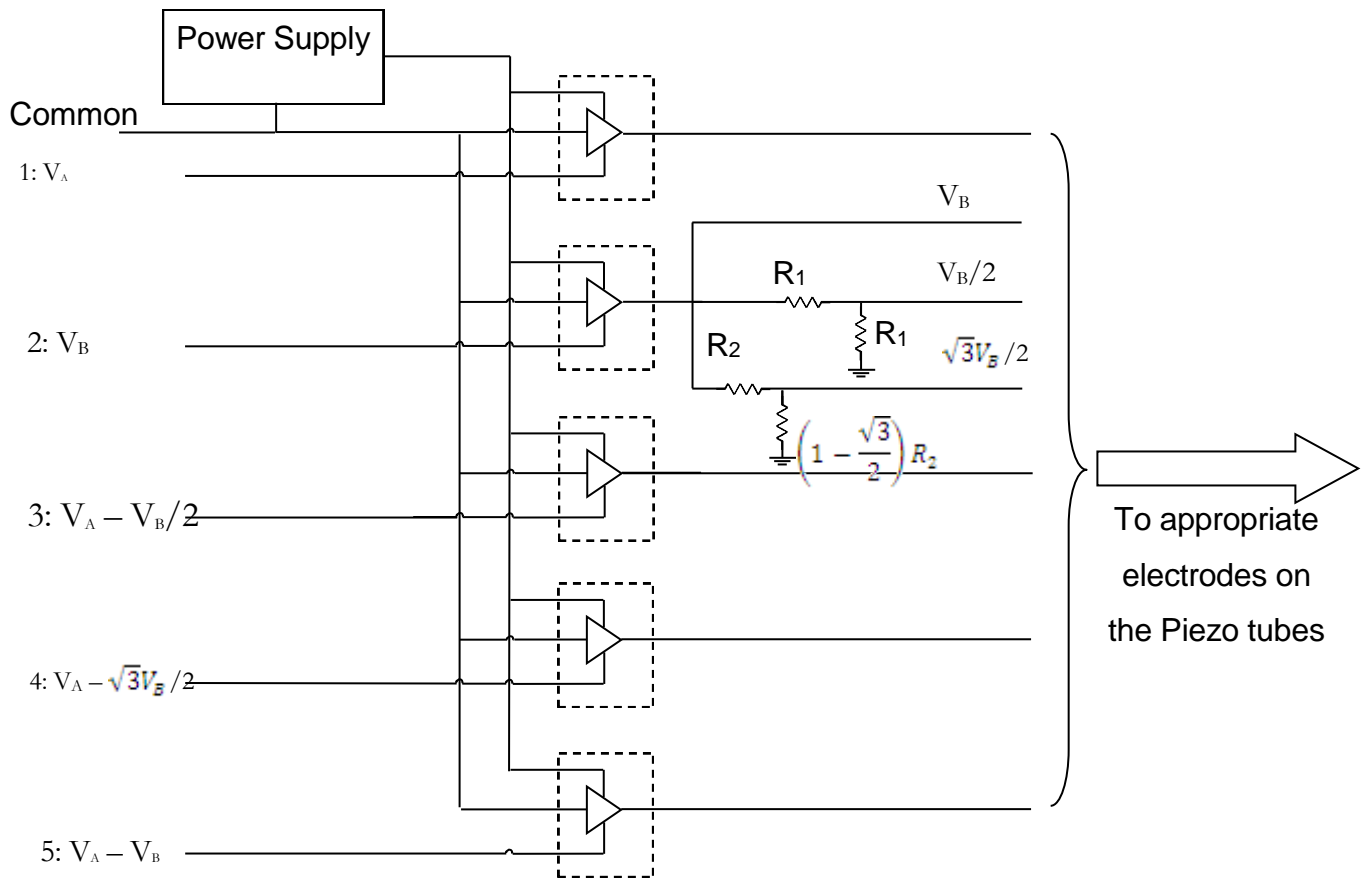


Figure 29. Schematic of the approach circuit. The computer outputs signals which have already been divided (compared to the signals for the scanning mode). However, in order to have seven different potentials, resistors are used to divide the second voltage, as shown. The seven resulting potentials are then attached to the appropriate electrodes on the piezos, as shown in Figure 28.

Chapter 4

CONCLUSION

4.1 Summary

The AFM, first invented in 1985, is a valuable tool for probing the nature of matter, especially for examining the surfaces of insulators. A variable temperature AFM will provide even more information about materials. The variable temperature AFM described in this thesis utilizes an inverted Johnny Walker sample mount and a laser deflection detection system. Piezos are used both for movement of the sample and for oscillations of the tip. All materials used in construction are carefully chosen and placed so that measurements will be possible during heating and cooling. A LabVIEW program is being developed to run the microscope and store the data.

4.2 Future Work

While much progress has been made on this project, there remains more to be done before imaging of surfaces can take place. Future work will first require successful tests of the program and the electronics for the approach mode must be completed. This mode is more easily testable than the scanning and positioning modes since motion in this mode is on a slightly larger distance scale. Successful completion of the testing of this portion of the project will direct the further development of the rest of the program and electronics.

The laser system and the heating and cooling systems will then need to be built. Since the laser generates thermal energy and is affected by the temperature of its environment, these two components must be considered together.

Once all the features described in this paper are functioning, the AFM will be placed in a rough vacuum system to increase the resolution of the images.

Appendix

LABVIEW PROGRAM

4.3 Introduction

The appendix presents the labview code in its current state of development. The front panel and block diagram of each section of the program are shown, with relevant notes. The block diagrams for subVI's are included where appropriate.

4.4 Menu.vi

This program provides a user interface for accessing all modes of operation. Event structure is utilized. As discussed above, this portion of the program is still in an early stage.

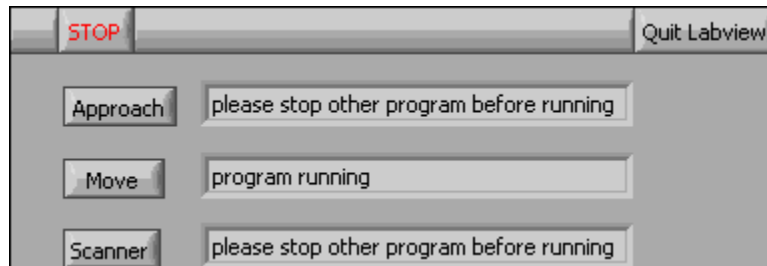


Figure 30. Front panel for Menu.vi. The text changes whenever one of the programs is in operation. The programs are not designed to run at the same time, since this is not physically possible anyway. The goal of the Menu program is to provide an easy interface from which the user can control all necessary aspects of the program and switch between the modes of operation.

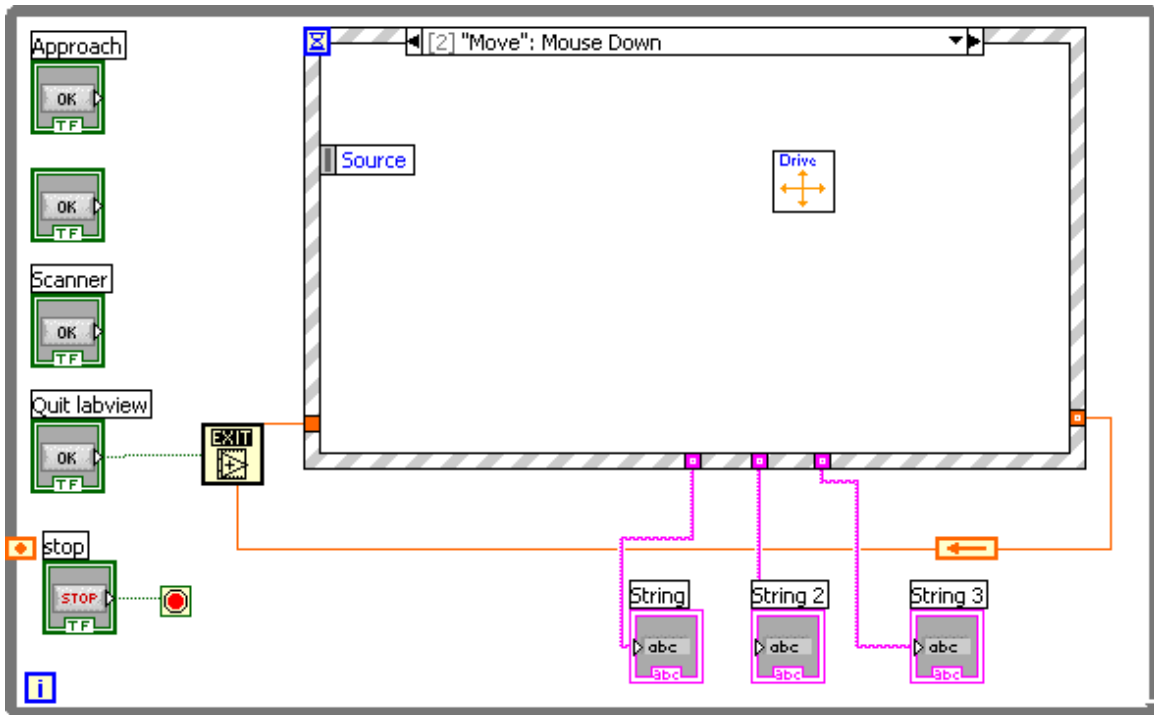


Figure 31. Block diagram for Menu.vi. The pressing of each button corresponds to an event case. Each of the event cases opens the corresponding program in a new window. The event cases are shown below.

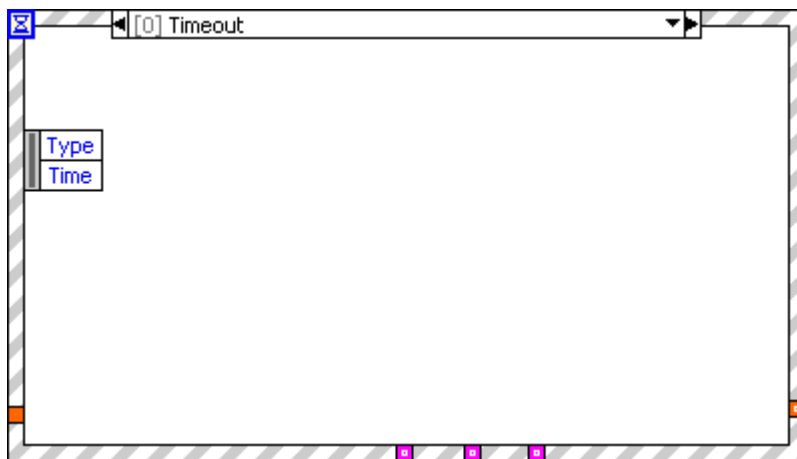


Figure 32. Event case for the event structure shown in Figure 31. The timeout case is a default part of the event structure.

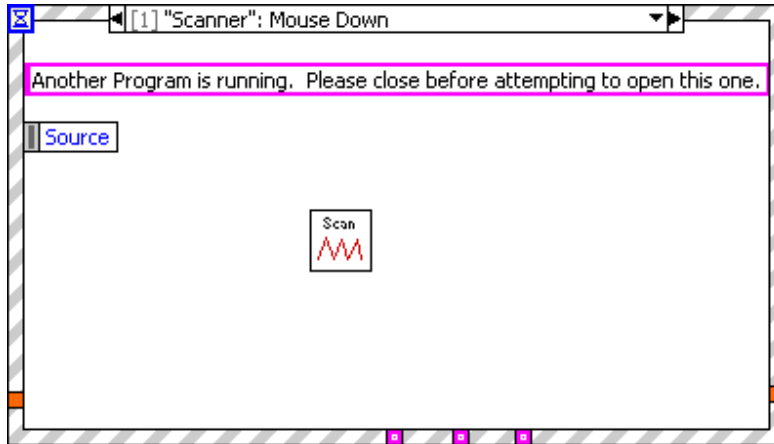


Figure 33. Event case for the event structure shown in Figure 31. This case opens the Scanner program.

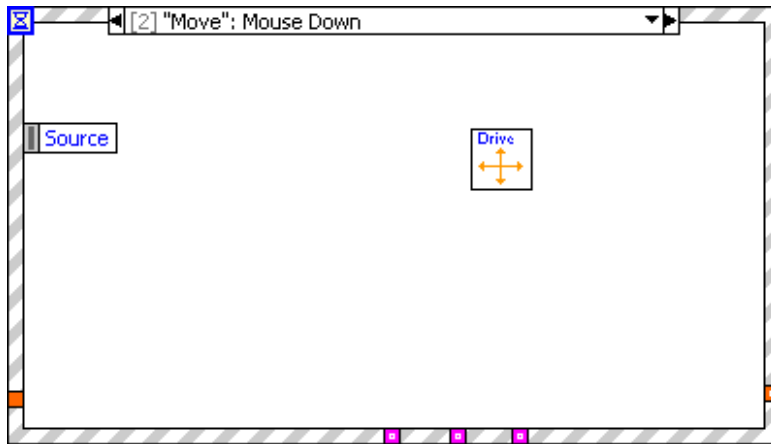


Figure 34. Event case for the event structure shown in Figure 31. This case opens the Drive program, for fine-tuning the position.

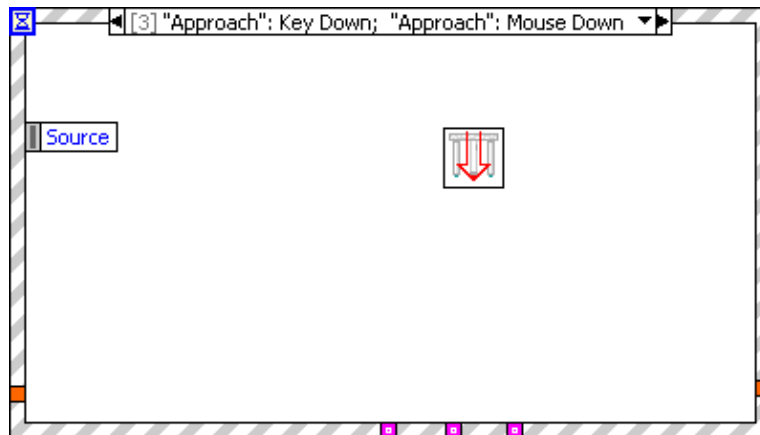


Figure 35. Event case for the event structure shown in Figure 31. This case opens the Approach program, for moving the sample mount up or down in slip-stick motion.

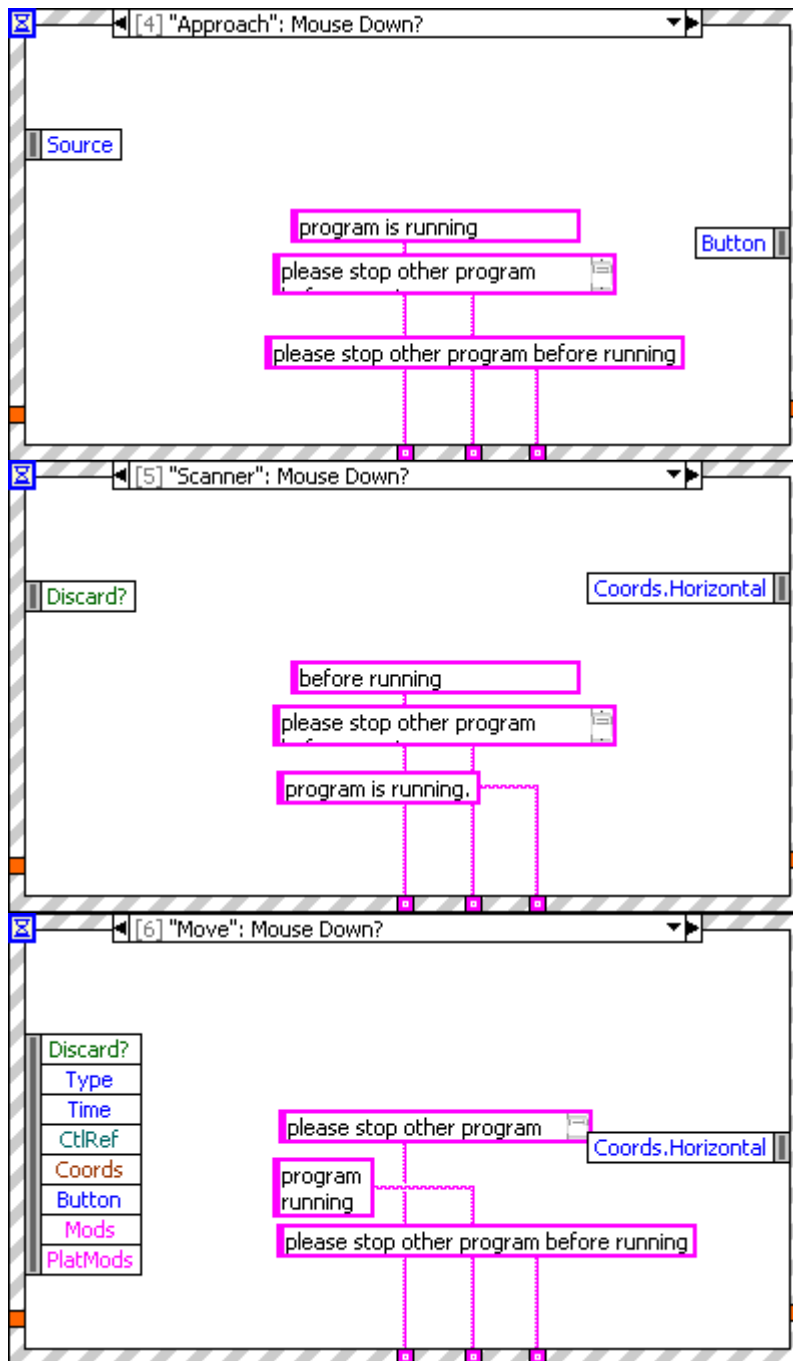


Figure 36. Event cases for the event structure shown in Figure 31. These event cases control the strings which appear in the text boxes.

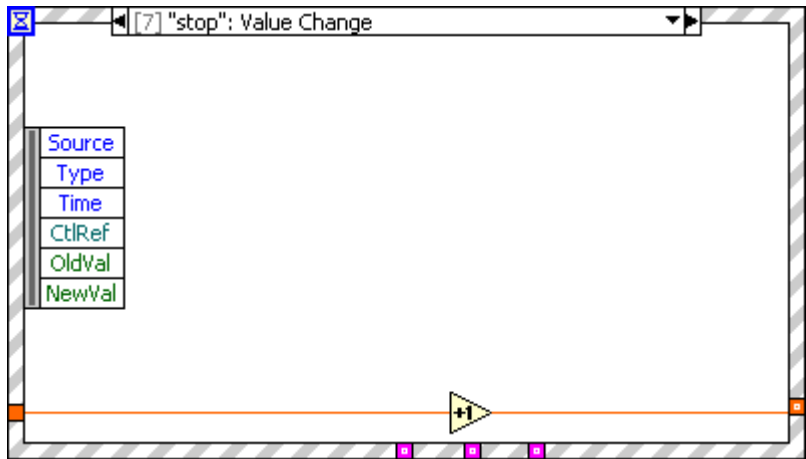


Figure 37. Event case for the event structure shown in Figure 31. This event case executes when the stop button is pressed, enabling the program to end (otherwise it would wait until some other event case had been executed).

4.5 Approach.vi

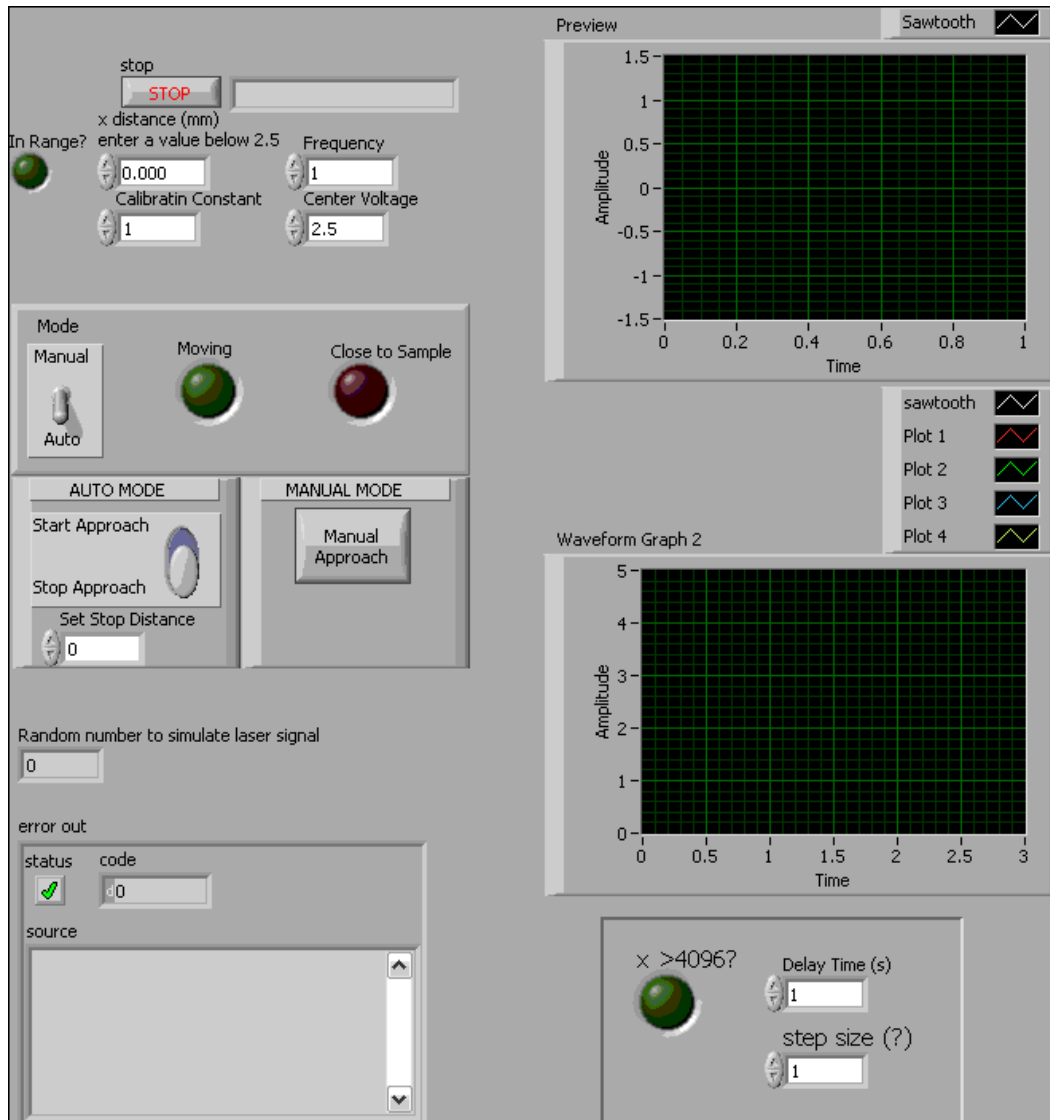


Figure 38. Front panel for the approach sub program, Approach.vi. The user inputs values for the step size and frequency of step. The step size will be coerced to the maximum value if the output voltage is not within the 1-5V range. The calibration constant will be useful for tuning the microscope, so that the calibrated step size will correspond to a physical distance.

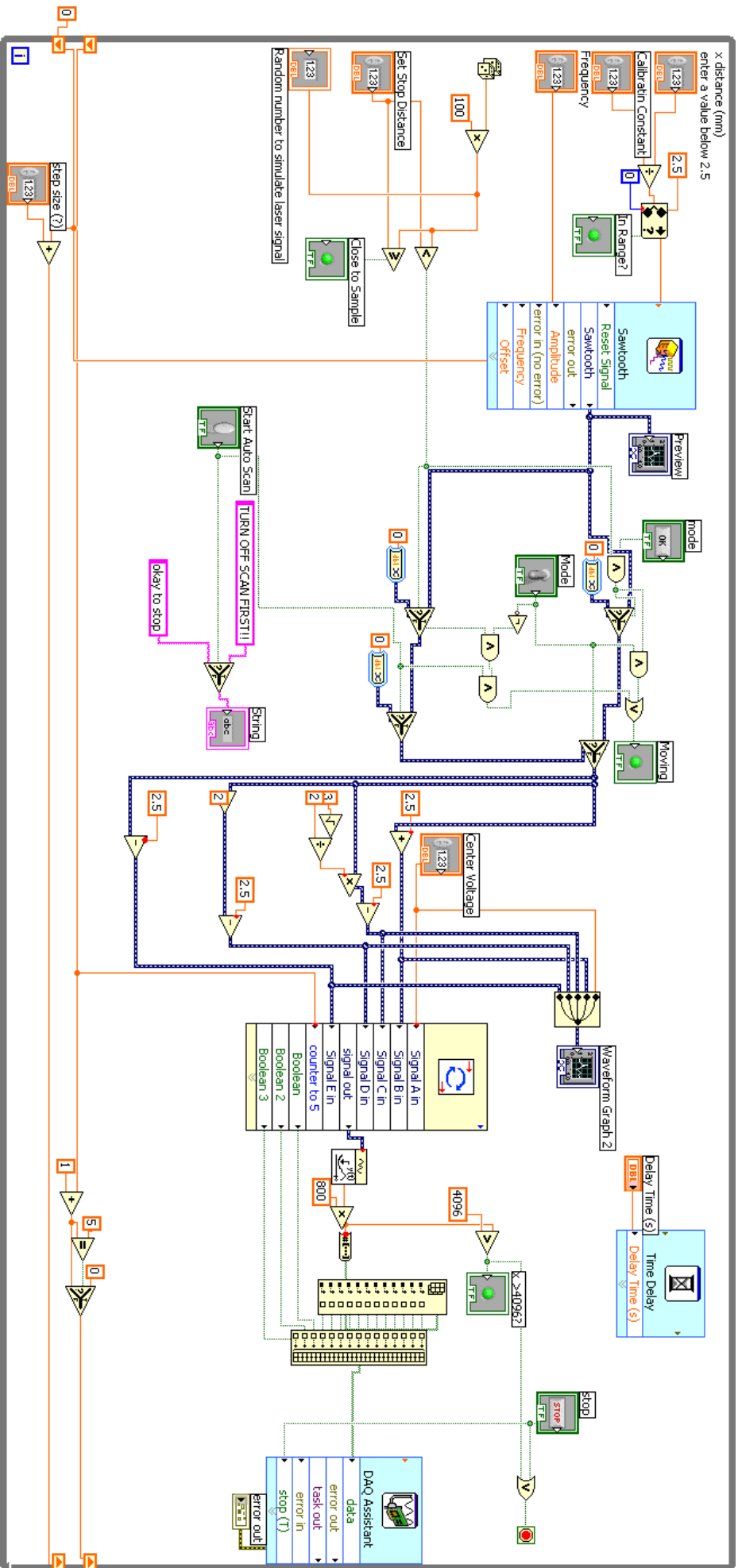


Figure 39. Block diagram for Approach vi. The logic is described in Section 3.5.1. A random number generator is used to simulate the laser signal, until a signal can be obtained.

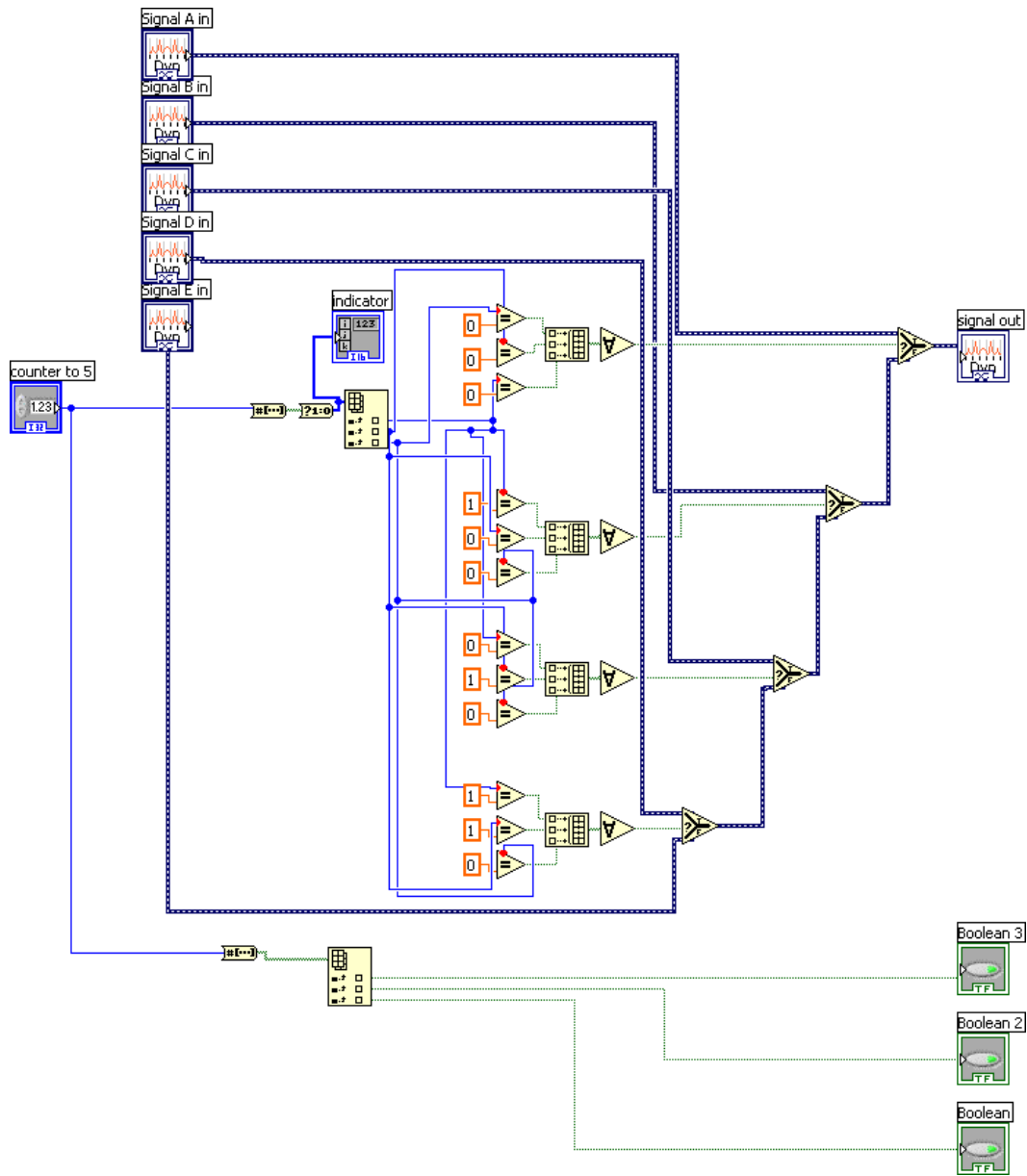


Figure 40. Cycle subvi. The larger program was simplified by creating a subvi which would perform the cycling through action. Five signals are input into this program. These signals are then output one and a time, in order, each time the program executes. This continues on indefinitely until the structure in which it is placed is stopped. The Boolean outputs are used as addresses, to separate the signals out again in the electronics.

4.6 Positioning.vi

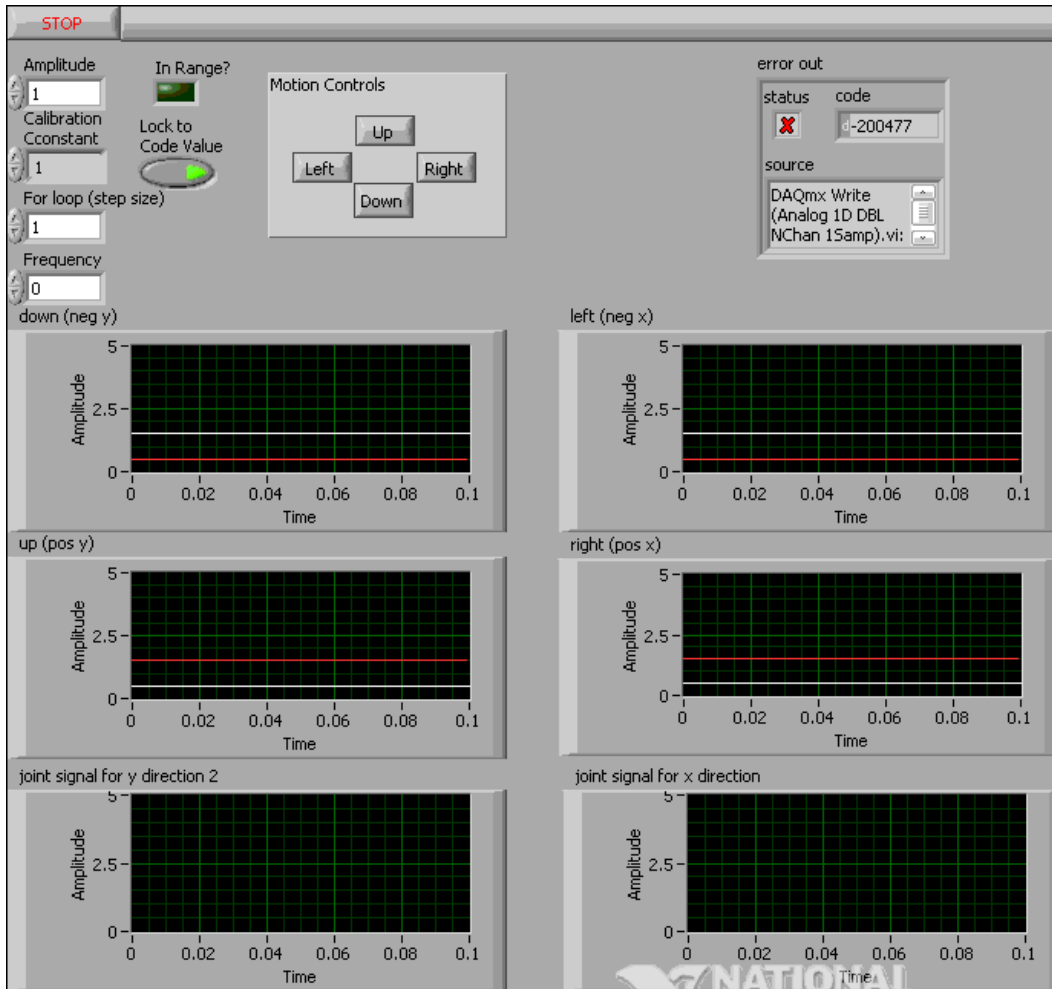


Figure 41. Front panel for Positioning.vi. User specifies amplitude of motion. The calibration constant can be used in initial calibration, and then locked. The user also specifies the number of steps for every time a motion control is pressed, and the frequency of those steps. Keyboard shortcuts allow the user to operate the microscope from the keyboard. However, care must be used with this method, since holding down a key in any one direction may result in an overload or a lag, causing the signals to be sent after the user had intended them to be.

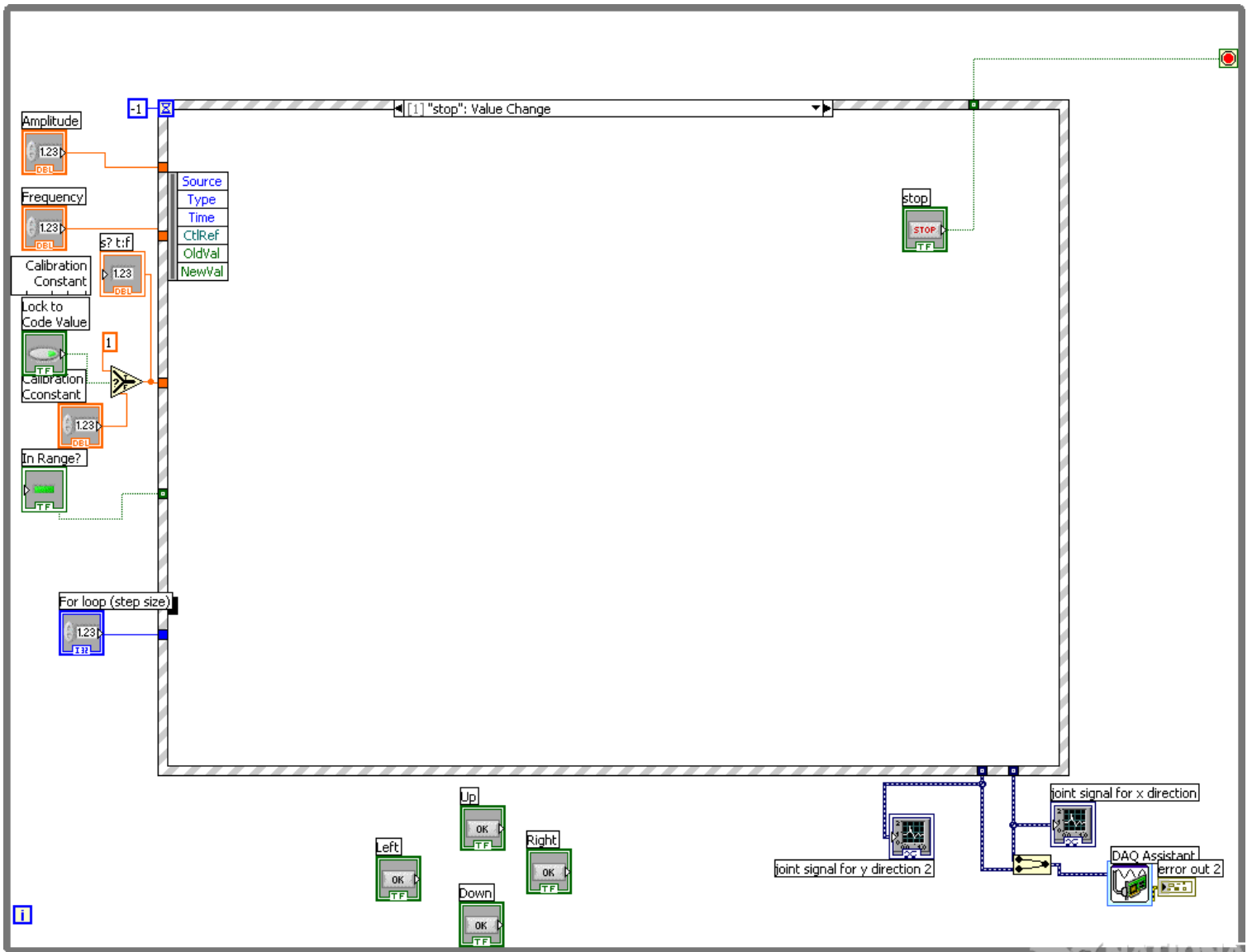


Figure 42. Block diagram for Positioning.vi. Event structure is utilized. A center voltage output and cycling through capabilities will be added after these features have been tested.

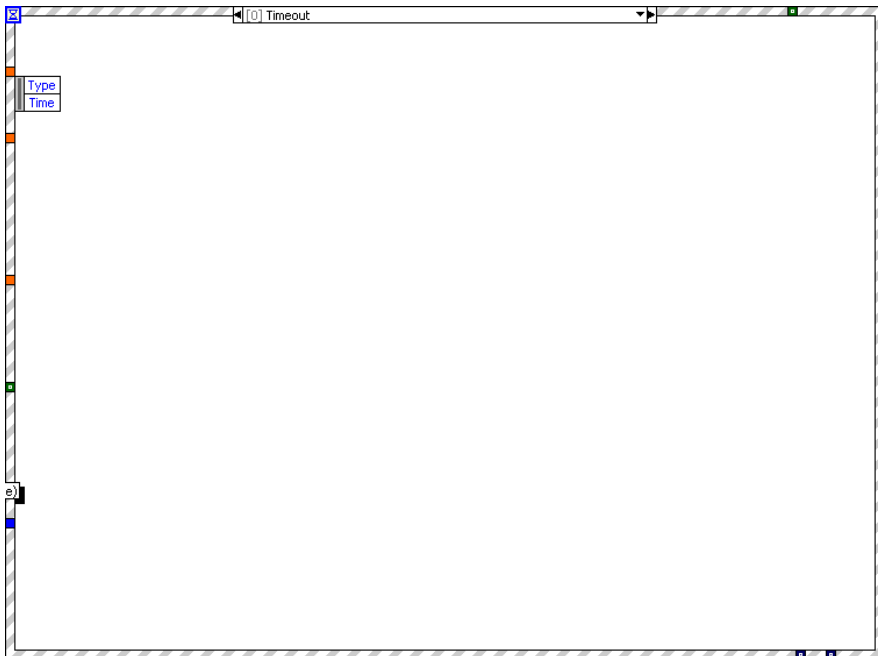


Figure 43. Event case for Positioning.vi. This is the default timeout case for the event structure.

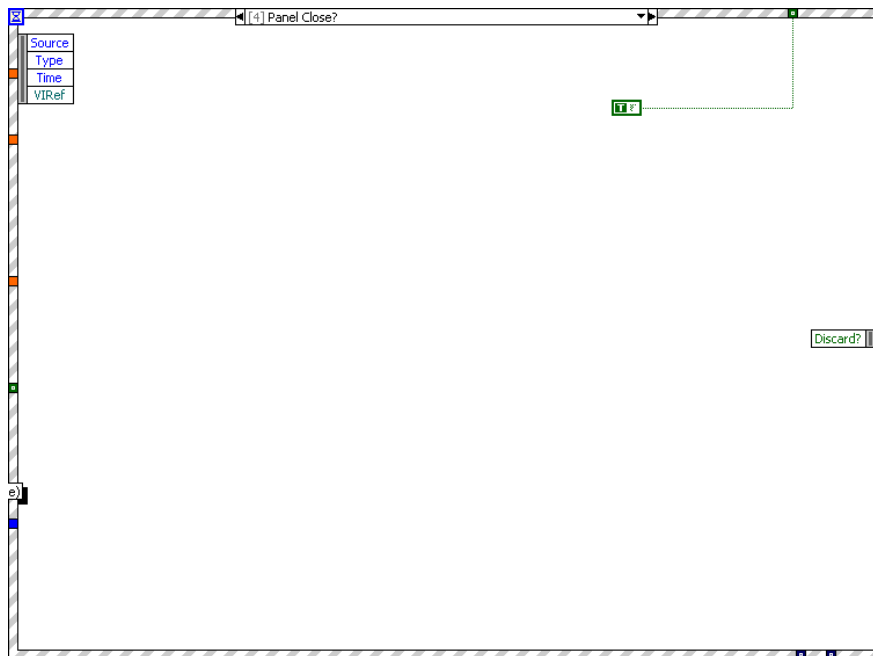


Figure 44. Event case for Positioning.vi. This case causes the program to end normally when the panel is closed by the user.

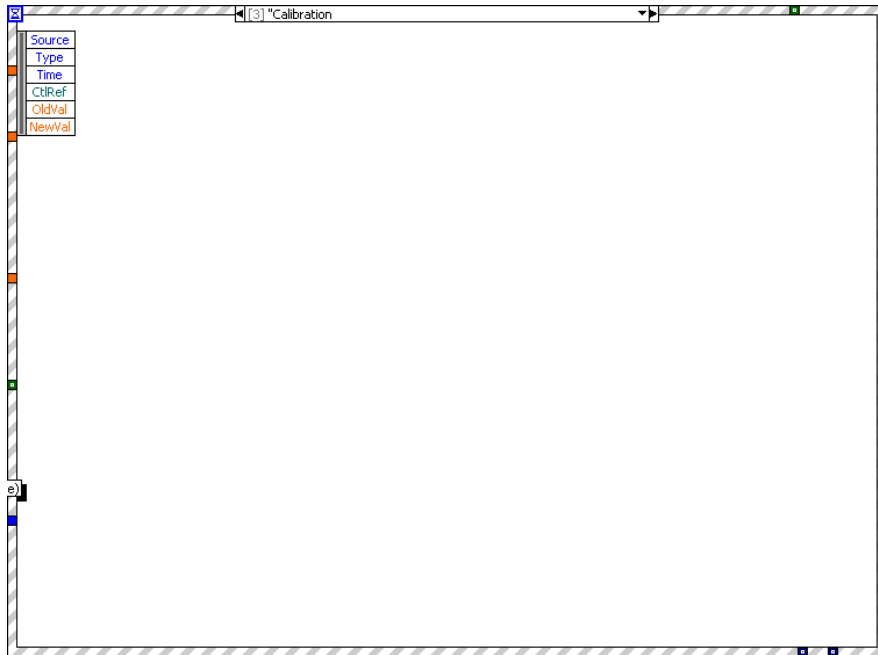


Figure 45. Event case for Positioning.vi. This event case causes the structure to completely execute when the calibration is adjusted.

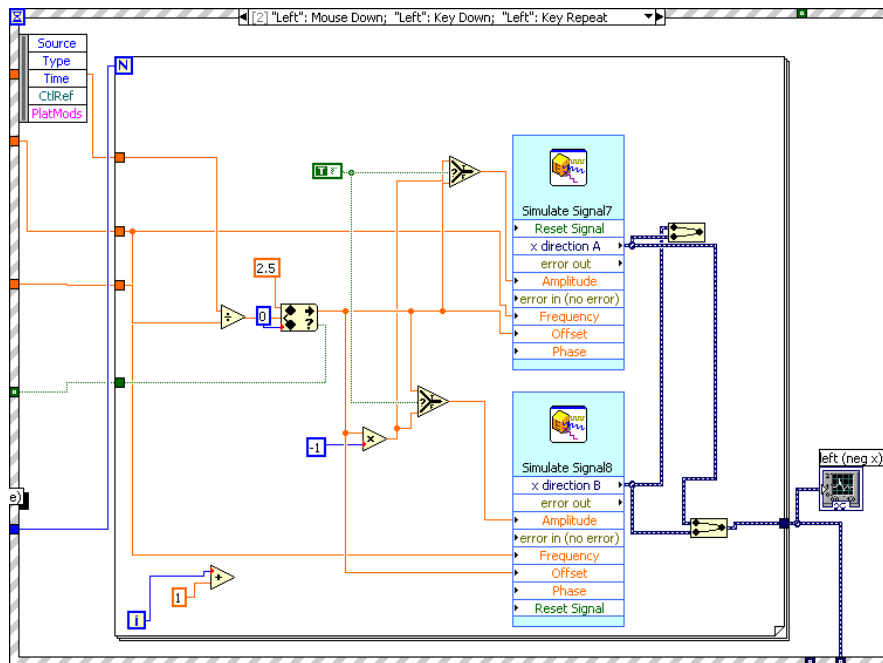


Figure 46. Event case for Positioning.vi. This is the event case for motion in the negative x direction. Two functions are generated, one being the opposite of the other.

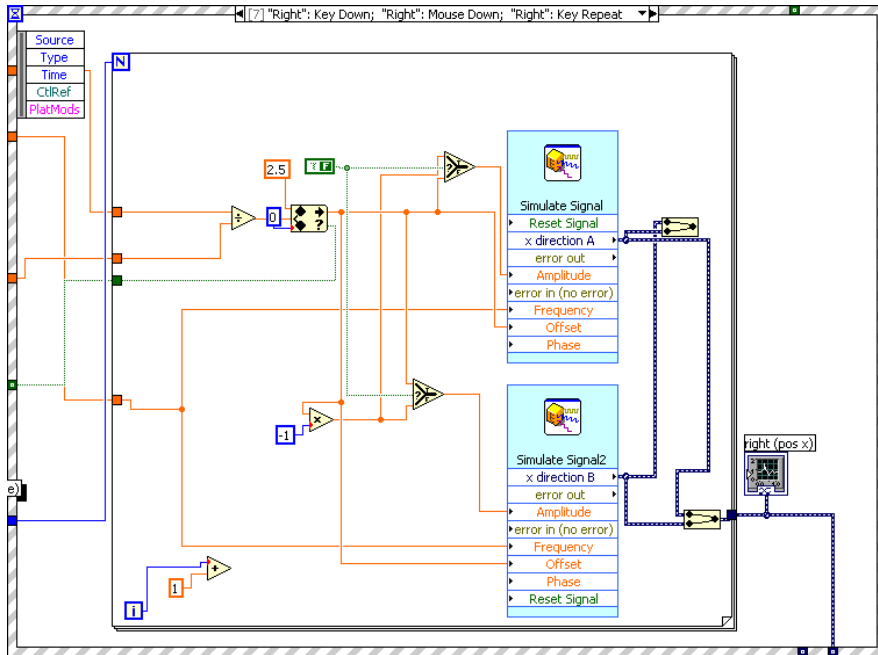


Figure 47. Event case for Positioning.vi, for motion in the positive x direction. Two functions are generated, one being the opposite of the other. The only difference between this case and the previous one is the true-false constant, which determines which function is negative of the other. This causes the piezo tubes to bend the opposite direction.

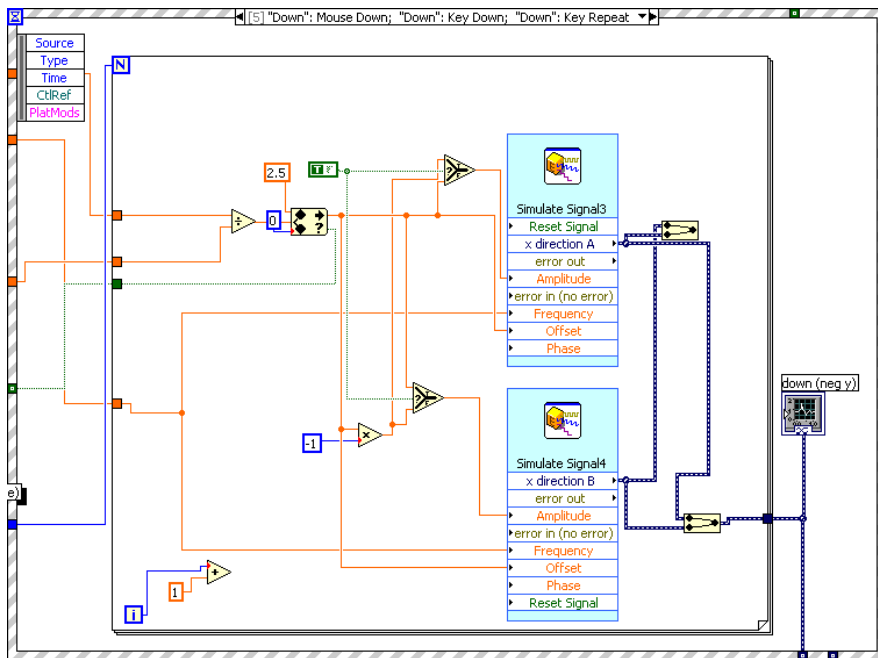


Figure 48. Event case for Positioning.vi. This is the event case for motion in the negative y direction, and is identical to the one shown in Figure 46; the difference in direction of motion comes from wiring the output to a different electrode.

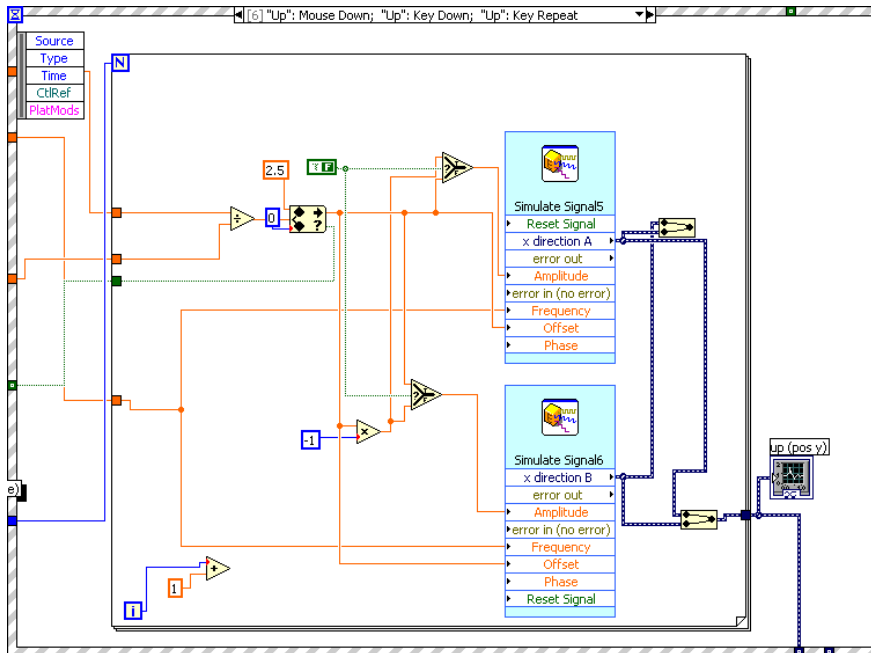


Figure 49. Event case for Positioning.vi. This is the event case for motion in the positive y direction, and is identical to the one shown in Figure 47; the difference in direction of motion comes from wiring the output to a different electrode.

4.7 Scanning

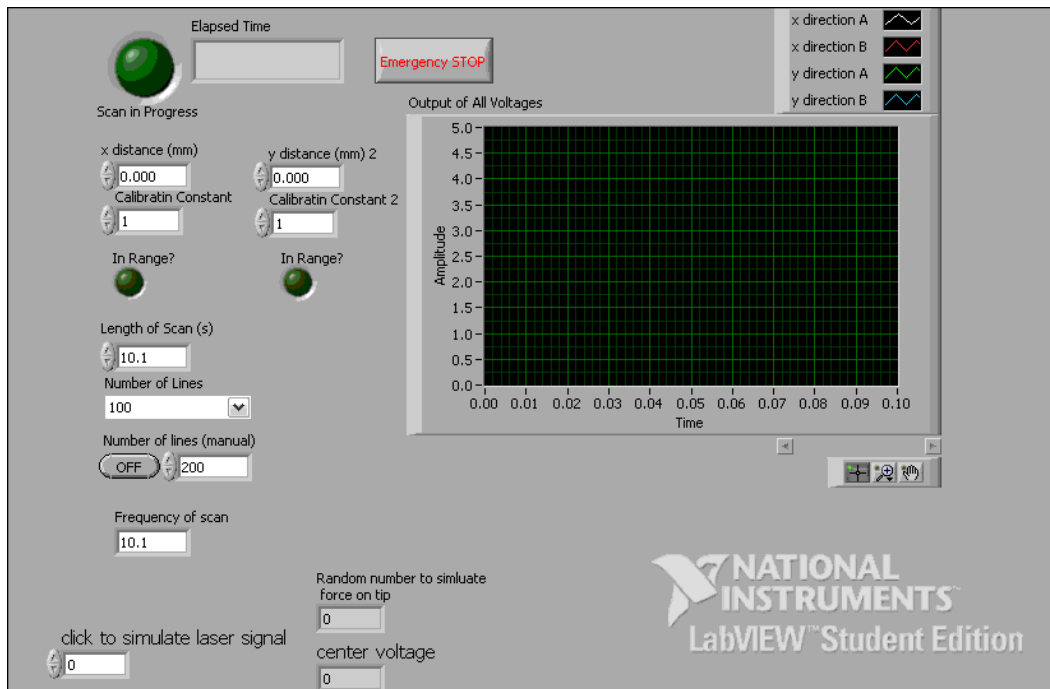


Figure 50. Front panel for Scanning.vi. The user specifies the resolution of the scan by indicating the number of lines (number of times back and forth) and the size of the region to be scanned. The speed of the scanning is also specified. Once the scan has begun, a light turns on and an indicator specifies the elapsed time.

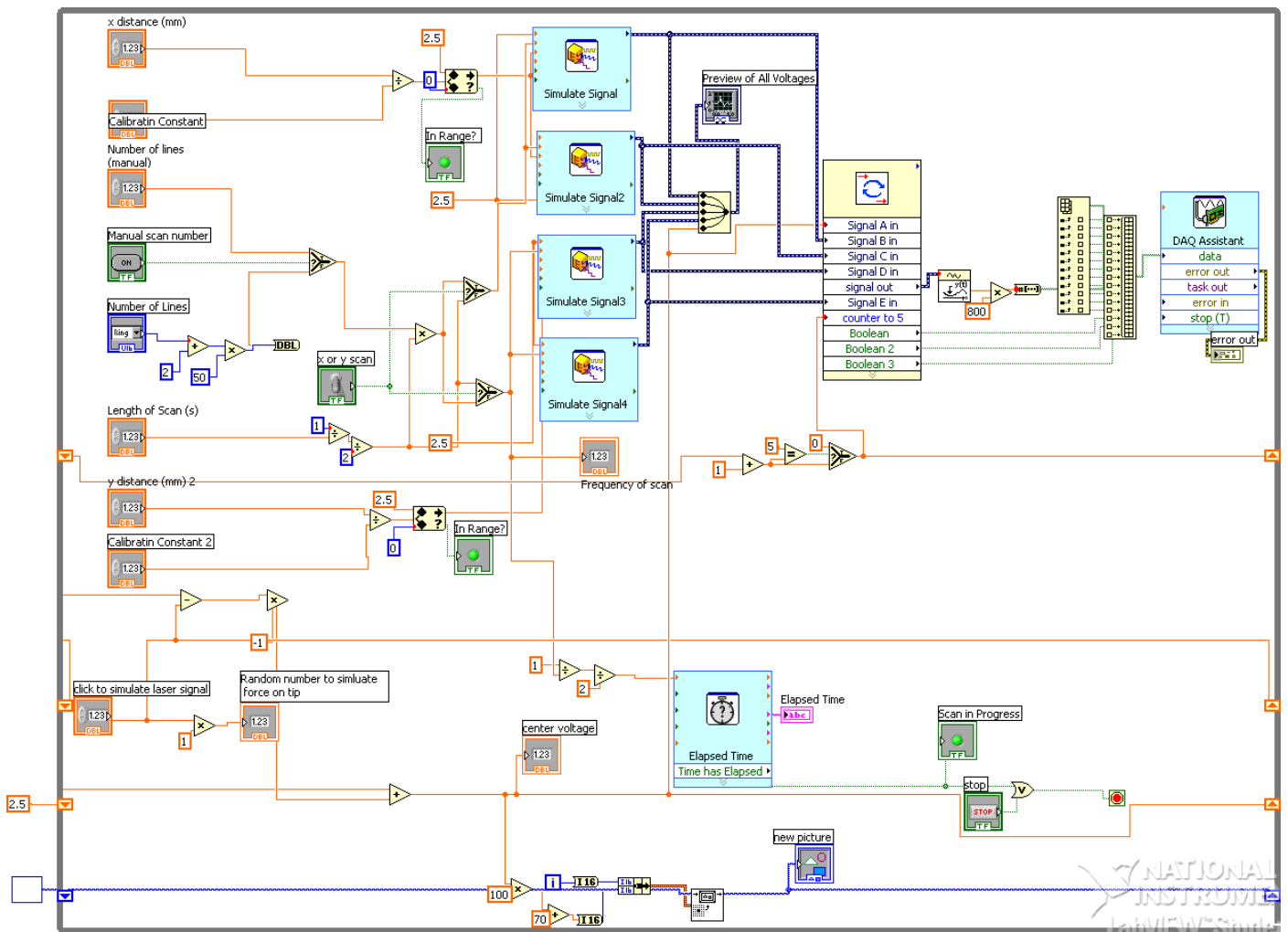


Figure 51. Block diagram for Scanning.vi. Four triangle waves are generated and out put to a plot and to the cycle subvi. This subvi is the same as the one shown in Figure 40. The same signal conversion technique as in Figure 39 (Approach) is used. The Elapsed Time express vi counts off the time input into it and then sends a Boolean signal when the time has elapsed. This Boolean value is then wired to the stop for the while loop structure. The portion of the program at the very bottom of the loop is for testing purposes; the output values are converted into points on an image, with each subsequent point being plotted further to the right so that the output voltage can be mapped as a function of time.

REFERENCES

- [1] G. Binnig, C.F. Quate and C. Gerber, *Phys. Rev. Lett.* **56**, 930 (1985)
- [2] P. E. West, *Introduction to Atomic Force Microscopy: Theory, Practical Applications* (Pacific Nanotechnology, inc, Santa Clara, 2002-2009), p. 4.
- [3] R. Young *et. al.*, *Rev. Sci. Instr.*, **43** (6), 999 (1972).
- [4] J. S. Townsend *A Modern Approach to Quantum Mechanics* (University Science Books, Sausalito, 2000) p.192.
- [5] G. Binnig and H. Rohrer, *Helvetica Physica Acta* **55**, 6, 726 (1982).
- [6] T.R. Albrecht and C.F. Quate, *J. Appl. Phys.* **62**, 2599 (1987).
- [7] M.H. Mahdavi *et. al.*, *Ultramicroscopy* **109**, 54 (2008).
- [8] A. Beiser, *Perspectives of Modern Physics*, (McGraw-Hill, New York, 1969), p. 400-402.
- [9] H. C. Hamaker, *Physica* **4** (10), 1058 (1937).
- [10] C. Argento and R. H. French, *J. Appl. Phys.* **80** (11), 6081 (1996).
- [11] V. Scherer *et. al.*, *Atomic Force Microscopy with Lateral Modulation*, in: B. Bhushan, H. Fuchs, S. Hosaka (Eds.), *Applied Scanning Probe Methods*. (Springer-Verlag, Berlin, 2004), p.79-82.
- [12] P. E. West, *Introduction to Atomic Force Microscopy: Theory, Practical Applications* (Pacific Nanotechnology, inc, Santa Clara, 2002-2009), p. 74.
- [13] P. E. West, *Introduction to Atomic Force Microscopy: Theory, Practical Applications* (Pacific Nanotechnology, inc, Santa Clara, 2002-2009), p 73.
- [14] F. Tian *et. al.*, *Ultramicroscopy* **109**, 45 (2008).
- [15] J. S. Villarrubia, *Tip Characterization for Dimensional Nanometrology*, in B. Bhushan, H. Fuchs, S. Hosaka (Eds.), *Applied Scanning Probe Methods*. (Springer-Verlag, Berlin, 2004), p.147-168.
- [16] D. Sarid, *Scanning Force Microscopy* (Oxford University Press, Oxford, 1991), p.x.
- [17] Y. Martin *et. al.*, *J. Appl. Phys.* **61** (10), 4723 (1987).
- [18] B.A. Saltuk and J.A. Turner, *Rev. Sci. Instrum.* **78**, 043704 (2007).
- [19] M Startk *et. al.*, *AIP Conference Proceedings*, Volume 696, pp. 385-391 (2003).
- [20] D.V. Pelekhov *et.al.*, *Appl. Phys. Lett.* **72**, 993 (1998).
- [21] D. Rugar *et.al.* *Rev. Sci. Instrum.* **59**(11), 2337 (1988).
- [22] D. Sarid *Scanning Force Microscopy* (Oxford University Press, Oxford, 1991), p.39.
- [23] H.J. Butt and M. Jaschke, *Nanotechnology* **6**, 1-7 (1995).
- [24] Q. Dai *et. al.*, *Rev. Sci. Instrum.* **66** (11), 5266 (1995).
- [25] M. Allegrini *et. al.*, *Ultramicroscopy* **42**, 371 (1992).

-
- [26] G. Lippman, *Annales de chimie et de physique* **24** 145 (1881).
- [27] P. E. West, *Introduction to Atomic Force Microscopy: Theory, Practical Applications* (Pacific Nanotechnology, inc, Santa Clara, 2002-2009), p. 24.
- [28] K K. Leang, *IEEE Trans. on Control Systems Tech.* **15** (5), 927 (2007).